Polyhedron 241 (2023) 116469

Contents lists available at ScienceDirect

Polyhedron

journal homepage: www.elsevier.com/locate/poly

Synthesis, characterization, thermal, DFT study, antioxidant and antimicrobial in vitro investigations of indazole and its Ag(I) complex

Ceyhun Kucuk [a,*], Sibel Celik [b], Senay Yurdakul [c], Ebru Cotelı [b], Belgin Erdem [b]

[a] Ahmet Erdogan Vocational School of Health Services, Zonguldak Bulent Ecevit University, Zonguldak, Turkey
[b] Vocational School of Health Services, Kırsehir Ahi Evran University, 40100 Kırşehir, Turkey
[c] Department of Physics, Faculty of Science, Gazi University, Ankara, Turkey

ARTICLE INFO

Keywords:
Indazole
Antioxidant
Antimicrobial
Silver complex
DFT
Docking

ABSTRACT

In this study, experimental and computational analyses were performed on free indazole and its silver metal complex. By using spectral methods, thermal studies, and analytical analysis, a new synthesized Ag(I) complex has been characterized. The geometric structures were optimized, structural parameters were calculated, and the chemical reactivity of the synthesized compound was investigated using the DFT calculations. Topological (AIM, RDG) investigations were done to look into molecular properties in order to learn more about the complex's attractive bonds and van der Waals interactions. The antioxidant activities of indazole and its silver metal complex were determined in vitro using the DPPH (2,2-diphenyl-1-picrylhydrazyl) method. Ascorbic acid and BHT (butylatedhydroxytoluene) were used as the standard substances. As a result, it was determined that the antioxidant capacity of the indazole substance was higher than the Ag (I) complex. The antimicrobial activity of the Ag(I) complex against both Gram-negative and Gram-positive bacteria was superior to that of the free ligand. The result analyses were supported by molecular docking approaches to explore the possible interaction of each compound with anti-microbial and antioxidant agents.

1. Introduction

Free radicals are high-energy atoms or molecules with one or more unpaired electrons in their outer orbitals [1,2]. Free radicals are all important components of cells such as lipids, proteins, DNA, carbohydrates, and enzymes [3]. Therefore, it has become important to research and develop compounds with higher antioxidant activity for the treatment of injuries and diseases caused by free radicals. Indazoles are aromatic heterocyclic organic compounds. Indazole and its derivatives have a variety of biological activities [4]. Especially in recent years, studies have focused on the investigation of the broad bioactivities of indazole derivatives in concentrated form [5,6]. The ring systems of indazole and its derivatives contribute to the formation of many drug molecules. Therefore, they are pharmacologically important compounds. These drug molecules are granisetron, a 5HT3 receptor antagonist and antiemetic, analgesic, antipyretic, anti-inflammatory, anticancer, antiviral, and antimicrobial, and have been reported to exhibit antispermatogenic activity [7–12]. It has been reported that indazole and indazole-based compounds have antagonistic effects on the glucagon receptor [13] and the thrombin receptor [14]. In addition, 7-Nitroindazole (7-NI) is a strong hydroxyl radical (OH) and has been reported to be a cleaner [15]. In the treatment of cancer, indazole and its analogs are especially important [16,17]. Tetrahydroindazole and its derivatives have been obtained synthetically. Studies have shown that this substance has good antioxidant properties. [18–21]. In addition, it has been reported that synthetically prepared indazole derivatives have many biological and pharmacological properties [22]. In particular, Bendazac is a non-steroidal anti-inflammatory. It is used as an anti-cataract drug. It investigated whether 7-nitro indazole and its derivatives could be used in alcohol treatment. As a result of the research, it was concluded that these compounds are non-narcotic, analgesic, and antipsychotic drugs [23]. It has been noted that the toxicological side effects of silver, a bioactive species [24] with low toxicity, are less severe when it complexes with organic compounds [25]. Silver metal complexes can interact with proteins and enzymes, bind to or cleave DNA sequences, and more [26]. Silver metal compounds have shown promise as potential antimicrobial agents [27,28], anti-inflammatory candidates [29], and chemotherapeutic agents [27,28,30–32]. Additionally, transition metal complexes demonstrated significant antioxidant activity (HO, O2, etc.). Meanwhile, the synthesis of silver complexes [33] is used

* Corresponding author.
E-mail address: ceyhun.kucuk@beun.edu.tr (C. Kucuk).

https://doi.org/10.1016/j.poly.2023.116469
Received 3 March 2023; Accepted 19 May 2023
Available online 26 May 2023

to create potential drug molecules as well as test their suitability for homogenous catalysis, which is used to create new compounds by activating C—C and C—N bonds [34]. Based on the benefits of silver(I) and the emerging challenges in disease treatment, there is great interest in the development of new silver metal compounds with high pharmacological activity. This is part of a larger effort to develop new drugs to complement existing drugs and increase the fight against disease [35]. In particular, the development of the use of silver metal ions in a new fluorescent-based detection technology has been considered important due to desirable properties such as high selectivity, high sensitivity, real-time imaging, and easy manipulation both in vitro and in vivo in recent years, [36]. Additionally, compared to the free ligand alone, the metal complexes can insert and stack between DNA base pairs more readily and profoundly, which ultimately results in cell death. In this regard, it may open up new avenues for cancer therapy and diagnosis in the future.

In this study, the silver metal complex of indazole [$Ag(indz)_2NO_3$] was synthesized and characterized by elemental analysis, ^1H NMR, ^{13}C NMR, FT-IR, UV–Vis, mass spectroscopy, and thermogravimetric analysis methods. The structural and spectroscopic properties of indazole and its silver complex are investigated in order to correlate experimental and computational theoretical studies. The DFT computational approaches and applications were successfully used for the structure determination of the ligand and its Ag(I) complex, and then the spectroscopic characterization and comparison with the observed data. The theoretical calculations, such as electronic, nonlinear optical, and thermodynamic properties, and topological (AIM, RDG) analyses were performed. In addition, the thermal behavior of the Ag(I) complex in terms of DSC/TG were given. Further, the antioxidant capacity assay (DPPH) and antimicrobial activities of free ligand and the Ag(I) complex were studied in vitro. Molecular docking studies were also conducted to better understand the ligand's and its corresponding Ag(I) complex's molecular interactions with antioxidant and antimicrobial proteins.

2. Material and methods

2.1. Experimental methods

2.1.1. Synthesis of silver complex

Indazole (98% purity, with MDL Number: MFCD00005691) and silver nitrate (at 99% purity, with MDL Number: MFCD00003414) were supplied by Sigma-Aldrich Chemical Company. They were used in chemical synthesis and spectral analysis studies without further purification. Firstly, a 2 mmol solution of the indazole molecule in 20 mL of ethanol and a 1 mmol solution of $AgNO_3$ in 10 mL of ethanol were prepared. They were mixed separately for about 30 min at 50 °C using a magnetic stirrer. Then, the prepared $AgNO_3$ solution was gradually added to the indazole solution. The mixture was stirred for 3 h at 50 °C to allow the chemical reaction to take place without allowing the solvent to evaporate, and then the mixture, prepared at room temperature, was stored for one week, wrapped in aluminum foil, and not exposed to light. After one week, it was kept at + 4 °C for three months [37]. The synthesized chemical has a 78% yield. The ligand-to-metal ratio in the produced chemical is 2:1. For elemental (C, H, and N) analyses, the following experimental and calculated values were reported: [$Ag(C_7H_6N_2)_2NO_3$], CHN Exp: C: 41.40 %, H: 2.14 %, N: 16.80 % and, Calc: C: 41.40 %, H: 2.84 %, N: 17.24 %.

2.1.2. DPPH antioxidant activity

Pure indazole and $AgNO_3$ salts were used in this study (Merck). In addition, the DPPH radical (Merck) was used to assess antioxidant capacity. The chemicals used are of the highest analytical purity.

The free ligand indazole and its Ag complex were tested for antioxidant activity in vitro using the DPPH (2,2-diphenyl-1-picrylhydrazil) free radical scavenging method described in a previous paper [38]. Methanol was used to make a DPPH solution with a concentration of 0.1 mM. Aluminum foil was wrapped around the prepared DPPH solution. Samples at three different (25, 50, and 100 μg/mL) concentrations were prepared from indazole, indazole Ag(I) complex, standard BHT, and ascorbic acid. 1 mL of each of these prepared samples was taken and placed in test tubes. The tubes were then filled with 3 mL of a 0.1 mM DPPH solution. At room temperature, the absorbances of all samples were measured at 517 nm for 0 min, 30 min, 3 h, and 24 h using a UV–visible spectrophotometer (SP-3000 + OPTIMA). All of the samples tested were measured in triplicate, and the results were expressed as the mean standard deviation. The following equation was used to calculate the percent radical scavenging activities of the samples:

$$\%\,\text{Radical scavenging activity} = \frac{\text{Control Absorbance} - \text{Sample Absorbance}}{\text{Control Absorbance}} \text{x} 100 \quad (1)$$

In addition, the IC_{50} values of all samples prepared at 25, 50, and 100 μg/mL concentrations were calculated.

2.1.3. Antimicrobial scanning

The following 10 microorganisms, consisting of 9 bacteria and 1 yeast, were studied: *Staphylococcus aureus* (ATCC 25923), *Bacillus cereus* (709 Roma), *Bacillus subtilis* (ATCC 6633), *Enterococcus faecalis* (ATCC 29212), *Escherichia coli* (ATCC 25922), *Aeromonas hydrophila* (ATCC7966), *Pseudomonas aeruginosa* (ATCC 27853), *Vibrio anguillarum* (ATCC 43312), *Klebsiella pneumoniae* (ATCC 13883) and *Candida albicans* (ATCC 90028).

The antimicrobial activity of free ligand and its Ag(I) complex were assessed in vitro using the agar-well diffusion method [39]. The synthesized compound stock solution (10 mg/ml) was made by dissolving it in dimethyl sulfoxide (10 % DMSO). The suspensions were adjusted to 0.5 McFarland standard turbidity, and the bacteria were cultured in tripticase soy broth (TSB) at 37° C for 24 h. After that, sterile trpticase soy agar (TSA) was produced and put into Petri dishes. The agar was then given 1 h at 4 °C to solidify. The agar was punctured using sterile cork borers (6 mm). DMSO was utilized as a control, and 75 μl of the chemical solution was administered to the holes. *C. albicans* and the test microorganisms were grown at 37 °C for 18 to 24 h. At the end of the time period, the inhibition zones that had formed on the medium were measured in millimeters (mm). Tetracycline (10 mg/ml) and natamycin (30 mg/ml) antibiotics were used as positive controls.

The microtiter plate assay technique was used to calculate the minimum inhibitor concentration (MIC) of title compounds. The free ligand and Ag(I) complex compound were serially diluted at two-fold serial doses (512, 256, 128, 64, 32, 16.8, 4, and 2 μg/mL) before 1×10^6 CFU/ml of actively growing bacterial and yeast strains were introduced to the wells. Each well received 100 μl of tripticase soy broth [40]. The positive control consists of wells containing test strains injected with medium, while the negative control consists of wells containing media. The minimum inhibitory concentrations (MIC) of title compounds were established.

2.1.4. Test of quorum sensing inhibitions (QSI) of free ligand and its Ag(I) complex

The QSI activity of the free ligand and Ag(I) complex was evaluated using *C. violaceum* ATCC 12472. The inoculum included only colonies of *C. violaceum* ATCC 12472. At 28 °C with 200 rpm shaking, broth medium was used to develop Luria Bertani (LB). 15 mL of sterile trypticase soy agar (TSA) was placed onto the plates after being thawed at 55 °C. Following swab-spinning with 100 μl of *C.violaceum* ATCC 12472 culture, the plate was allowed to fully solidify before cork drill wells (7 mm in diameter) were drilled into the agar. Both compounds were dissolved in DMSO at a concentration of 5 mg/ml. 75 μl of the free ligand and Ag(I) complex were added to the agar wells. After 2 days of incubation at 28 °C, the amount of purple color around the well was measured, and its suppression was determined to be positive QSI activity. DMSO was used as a negative control [41].

2.1.5. Instrumentation for recording spectra and DSC/TGA measurements

Infrared spectra in the region of 4000–550 cm^{-1} and 45000–100 cm^{-1} were recorded using Bruker Vertex 80 FT-IR and Bruker IFS 66/S spectrometers, respectively. ^{1}H and ^{13}C NMR spectra were recorded using a liquid Bruker 400 MHz AV model NMR spectrometer with an operating frequency of 400 MHz in DMSO solution. An Agilent HP 8453 spectrophotometer was used to record the UV–Vis spectrum in a quartz cell using DMSO as the solvent in the range of 190–1100 nm. The mass spectrum of the Ag(I) complex was recorded with a Waters Synapt G1 model spectrophotometer using high-resolution mass spectrometry (HRMS) in the positive mode (ES +) range of 50–1000 Da. The differential scanning calorimetry thermogravimetry analysis (DSC/TGA) was performed in a dynamic N_2 atmosphere (40 mL/min) with a heating rate of 25 °C/min from a surrounding temperature of 1400 °C/min using a Mettler Toledo thermal analyzer.

2.2. Computational methods

The density functional theory (DFT) calculations were performed using GAUSSIAN 09 and visualized with the Gaussian View 5.0 program [42,43]. The geometric optimization, frequencies, electronic, optical, and thermodynamic properties of the indazole molecule are calculated using the 6–311++G(d,p) basic set with the B3LYP function in the DFT method [44], while the same properties for its silver nitrate complex structure are calculated by applying the combination of the 6–311++G (d,p) and the LanL2DZ basis sets [45]. Total energy distribution analysis for vibrational modes was performed by the VEDA program [46]. The theoretical UV–Vis values of the title complex were calculated in the DFT/B3LYP method using a combination of 6–311++G(d,p) (for C, N, H, and O atoms) and LANL2DZ (for Ag atom) basis sets. NMR calculations were performed with the GIAO method by using the 6–311 + G(2d, p) basis set for the free indazole molecule [47], and were performed using a combination of 6–311 + G(2d,p) and LanL2DZ for the [Ag $(indz)_2NO_3$] complex [48]. Multiwfn [49] and the molecular visualization program VMD [50] were used to determine the intensity of non-covalent interactions (NCIs), the isodensity surface plot, and the reduced density gradient (RDG) surface. Auto dock 4.2.6 Tools were used to construct the initial structures to run the docking simulations. The world's largest online protein database, RCSB, is the major source for collecting the PDB structures used as target proteins. The receptors of gram positive bacteria (*Staphylococcus aureus,* PDB ID: 5FPO), *Candida albicans* (PDB ID: 4LEB), and an antioxidant enzyme (PDB ID: 3MNG) were obtained from the RCSB Protein Data Bank (www.pdb.org) [51]. The docked poses were visualized using the Discovery Studio Visualizer [52] and USCF Chimera software [53].

3. Results and discussion

3.1. Molecular structure

The [Ag$(indz)_2NO_3$] complex was optimized using a combination of 6–311++G(d,p) (for C, H, and N atoms) and LanL2DZ basis sets (fort he Ag atom). The geometric parameters (bond length and bond angles) of the optimized structure are listed in supplementary Table S1, and these parameters are compared with the XRD parameters of indazole [54] and Bis(4,5-dihydro-1H-benzo[*g*]indazole) [55]. The optimized geometric structure of the title molecule is presented in Fig. 1. Also, the coordinates of the optimized geometry of the ligand and the Ag(I) complex were listed in the supplementary Table S2.

The lengths of the N_1-N_2 and N_{16}-N_{17} bonds in the pyrazole rings of the complex were calculated as 1.354 and 1.363 Å. The bond lengths of N_1-C_3, N_2-C_7, N_{16}-C_{18}, and N_{17}-C_{22} were also found to be 1.358, 1.325, 1.365, and 1.321 Å, respectively. The C_3-C_4 and C_4-C_7 bond lengths in the pyrazole rings were calculated as 1.419 Å, while C_{18}-C_{19} and C_{19}-C_{22} were calculated as 1.416 and 1.423 Å. While the benzene rings in the [Ag$(indz)_2NO_3$] complex have C—C bond lengths ranging from 1.379 Å to 1.423 Å. Five of the C—H bond lengths were found to be 1.083, two of them 1.084, and one of each 1.081 and 1.079 Å. The distances of N_2 and N_{17} atoms to Ag_{31} atoms were calculated as 2.236 and 2.244 Å, respectively. In addition, the distance of the Ag_{31} atom to the O_{32} and O_{33} atoms of the nitrate group was calculated as 2.735 and 2.531 Å. Finally, the O_{32}-N_{35}, O_{33}-N_{35}, and O_{34}-N_{35} bond lengths of the nitrate group were found to be 1.281, 1.270, and 1.223 Å.

When the geometric parameters of the newly synthesized [Ag $(indz)_2NO_3$] complex and the XRD data of previously studied Bis(4,5-dihydro-1H-benzo[*g*]indazole) are compared, the Ag-N, Ag-C, and N—O bond lengths in nitrate groups are quite compatible. Furthermore, with the exception of very small deviations, the bond lengths of the indazole

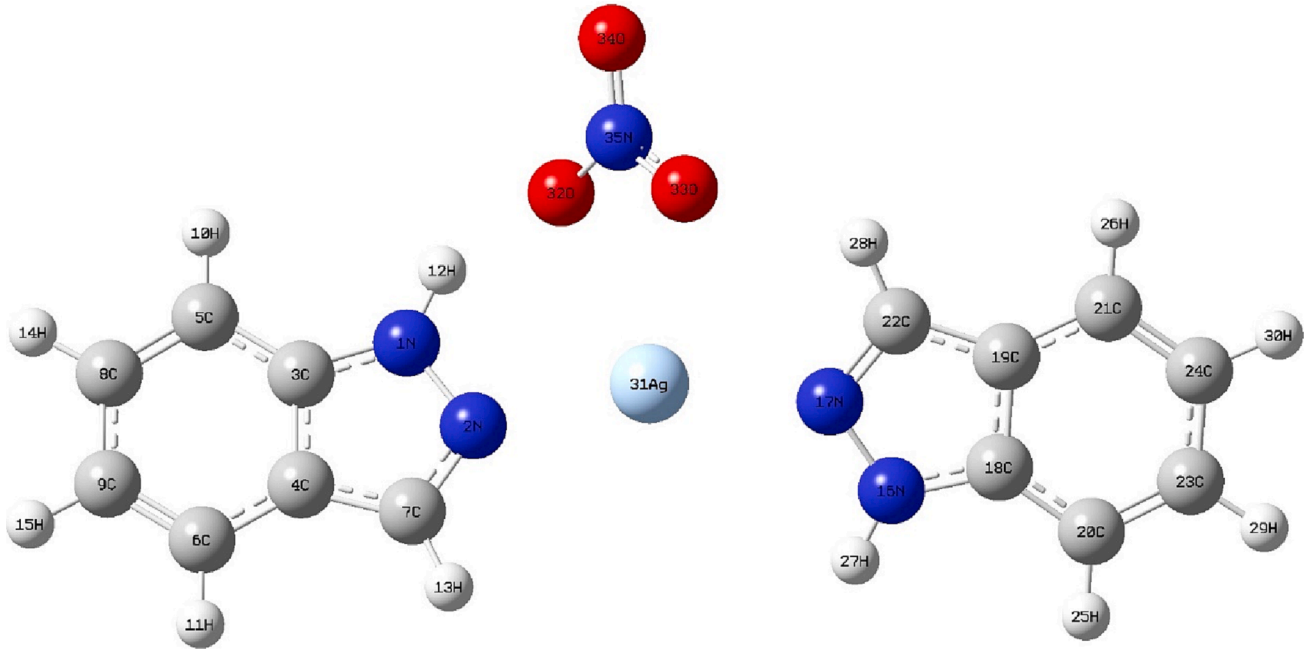

Fig. 1. Optimized geometric structure with atom numbering of the [Ag$(indz)_2NO_3$)] complex.

molecule in the complex structure are compatible with those of both 1H-indazole and Bis(4,5-dihydro-1H-benzo[*g*]indazole [55]. Finally, the bond angles of the title complex were compared with the both XRD data studied in the literature. The results were found quite compatible with the data of the 1H-indazole molecule [54]. In addition, when compared with the bond angles of Bis(4,5-dihydro-1H-benzo[*g*]indazole), it is seen that their bond angles are compatible except for C_7-N_2-Ag_{31}, N_1-C_3-C_5, and C_{22}-N_{17}-Ag_{31} [55]. The reason for the deviations determined for the bond length and bond angles is that the calculations are made in the gas phase without interactions in the crystal lattice, and the structures are not exactly the same.

3.2. Vibrational analysis

Modes assigned for the experimental and theoretical wavenumbers of the [Ag(indz)$_2$NO$_3$] complex were performed by accounting for the ≥ 10% total energy distribution (TED) contributions. Supplementary Table S3 presents scaled theoretical and measured wavenumbers of the Ag(I) complex as well as recorded wavenumbers of the indazole ligand. Scaling factors of 0.983 [56] and 0.961 [57] were used for wavenumbers below and above 1800 cm^{-1}, respectively. In addition, experimental Far-IR and FT-IR spectra of the indazole molecule and the [Ag(indz)$_2$NO$_3$] complex are presented in supplementary Fig. S1 and Fig. S2, respectively.

The N—H stretching vibrations of the heterocyclic molecules are expected to be observed in the region of 3500–3000 cm^{-1} [58]. These stretching vibrations of the [Ag(indz)$_2$NO$_3$] complex were observed at 3735 and 3154 cm^{-1} in the FT-IR spectrum and calculated at 3534 and 3182 cm^{-1}. These vibrational modes for the indazole molecule were experimentally observed at 3742 and 3148 cm^{-1}. According to these results, no significant change occurred in the experimental N—H stretching vibrations. The C—H stretching vibration peaks of hetero-aromatic molecules are observed in the region of 3100–3000 cm^{-1} [56]. These vibration values were observed at 3070 and 2930 cm^{-1} for the complex structure and at 3053 and 2917 cm^{-1} for the free ligand. Theoretical values corresponding to the experimental vibration values of the complex structure were calculated at 3109 and 3048 cm^{-1}. The other calculated C—H stretching vibration values of the Ag(I) complex were found to be within the required range.

The specification of C—N stretching vibrations is quite difficult, as different bands are also observed in this region. The C—N stretching vibrations of the Ag(I) complex were measured at 1630, 1446, 1372, 1353, and 1120 cm^{-1} in the FT-IR spectrum. The C—N vibrations for free ligand are seen at 1620, 1355, and 1122 cm^{-1}. The shift of the C—N vibration peak observed at 1620 cm^{-1} in the FT-IR of free ligand to a higher value of 1630 cm^{-1} in the spectrum of the complex indicates that the indazole molecule is involved in coordination with the silver metal. In a previous study, the C═N bands were measured at 1610 cm^{-1} for the free 2-chloroquinoxaline ligand and at 1540 cm^{-1} for both [Ag(2Cl-quinox)(NO$_3$)]$_n$ and [Ag(2Cl-quinox)$_2$(NO$_3$)]. In this study, the shift of the C═N bands to a lower frequency was reported as an indication of the coordination of silver metal and free ligand [59]. The theoretical C—N stretching wavenumbers corresponding to the experimental values of the title complex were also found to be 1636, 1444, 1397, 1358, and 1127 cm^{-1}. The ring C—C stretching vibrations are mostly seen between 1650 and 1200 cm^{-1} [47]. The C—C stretching vibrations for the complex structure were observed at 1630, 1508, 1120, and 999 g cm^{-1}. Also, these vibrations were calculated at 1636, 1518, 1127, and 1008 cm^{-1}. The other theoretical values of this vibration are given in Table S3. When these experimental vibrational values are compared with those of the indazole ligand, no significant shifts are observed, and they are quite similar to each other.

The band observed at 1355 cm^{-1} in the FT-IR spectrum of the free ligand was broadened and cleaved in the spectrum of the complex structure. The new peak that appeared at 1372 cm^{-1} of this broadened and cleaved band indicates the presence of the nitrate group that doesn't exist in the spectrum of the free ligand. Two strong Ag(I) complexes with quinoxaline ligand were synthesized and their FT-IR spectra were analyzed in the literature. The Ag atom is attached to two O atoms in the nitrate group of the synthesized [Ag(2Cl-quinox)(NO$_3$)]$_n$ and [Ag(2Cl-quinox)$_2$(NO$_3$)] complexes. The presence of a sharp spectral band at 1383 cm^{-1} was detected in the FTIR spectra of both synthesized complexes [59]. It was stated that these bands also show the presence of a nitrate group, which is not found in the FT-IR spectrum of the free ligand. For the [Ag$_2$L$_2$(NO$_3$)2]·H$_2$O complex (L: malonamide type ligand), a new band emerging at 1383 cm^{-1} is attributed to the N—O stretching vibration of the nitrate group [60]. In another study, a silver nitrate complex of 2-methylquinoxaline [Ag(2-MQ)(NO$_3$)] was synthesized. Similarly, in this study, the Ag atom bonds with two O atoms of the NO$_3$ group. In the frequency analysis part of this study, O—N vibration bands were observed at 1389 cm^{-1} in the FT-IR spectrum and at 1387 cm^{-1} in the FT-Ra spectrum [51]. In addition, two peaks of the N—O vibration for the title complex were observed at 1286 and 697 cm^{-1} in the experimental measurements and were calculated at 1481, 1260, 711, and 697 cm^{-1}. The N—O stretching vibrations of the [$C_{10}H_9N_3$]$_4$AgNO$_3$] complex were calculated at 1325, 1168, and 934 cm-1. Also, in that study, these vibration bands were observed at 1337 (FT-IR)/1334 (FT-Ra), 1196 (FT-IR)/1204 (FT-Ra), and 954 (FT-IR) cm^{-1} [62]. Another useful example is IR analyses for the synthesis of [Ag($N_2C_{11}H_{10}$)$_2$]NO$_3$ complex salt. In this synthesized structure, the Ag atom bonds with two O atoms of the nitrate group. In the theoretical calculations of this structure, the O—N vibration frequencies were found to be 1377.6, 959.8, and 720.5 cm^{-1}, respectively [55].

While stretching vibrations of the Ag-N bond were measured at 424 and 95 cm^{-1}, they were calculated at 426, 189, 178, 94, and 85 cm^{-1}. The peaks observed at 424 and 95 cm in the FT-IR spectrum of the complex are not found in those of the free ligand. These observed new spectral peaks indicate that the Ag(I) complex of the free ligand is formed. In the vibration analysis of the [Ag(methyl-4-pyridyl ketone)$_2$NO$_3$] complex, Ag-N stretching vibration values were found to be 368, 179, 164, 103, and 82 cm^{-1} in theoretical calculations. In experimental measurements, it was observed in the IR spectrum at 382, 190, 163, 102, and 76 cm^{-1}, while it was also observed at 364 and 84 cm^{-1} in the Raman spectrum [57]. In another study, the Ag-N stretching vibrations for the silver nitrate complex of 2-Methylquinoxaline were observed at 719 (IR)/704 (Ra), 271 (Ra), and 141 (IR) cm^{-1} and were computed at 711, 286, and 138 cm^{-1} [61].

Finally, a correlation graph was drawn for linear regression analysis to show the agreement between experimental and theoretical wave numbers of the complex structure with silver nitrate and was presented in supplementary Fig. S3. The equation and correlation constant R^2 obtained from this graph are as follows [63]:

$$\nu_{cal} = 1.0031\nu_{\exp} - 2.4772R^2 : 0.9978 \quad (2)$$

According to this R^2 value, there is a good harmony between the experimental and theoretical wavenumbers of the [Ag(indz)$_2$NO$_3$] complex.

3.3. ^{1}H and ^{13}C NMR analyses

^{1}H and ^{13}C NMR analyses of the indazole molecule and its Ag(I) complex were performed using theoretical and experimental methods. While the experimental chemical shift measurements were taken in DMSO, the theoretical calculations were carried out at the DFT/B3LYP level of theory and using the GIAO method. In addition, the 6–311 + G (2d,p) basis set [45] and a combination of the 6–311 + G (2d,p) and LanL2DZ basis sets [48] were used in calculations for the indazole molecule and the Ag(I) complex, respectively. The chemical shift values are listed in Supplementry Table S4, while the experimental and theoretical spectra are presented in Supplementary Fig. S4.

Experimental ^{1}H and ^{13}C NMR chemical shift values for the indazole

molecule are as follows: H_{10}(7.78), H_{11}(7.54), H_{13} (8.08), H_{14} (7.35), and H_{15} (7.10) ppm, and C_3 (140.14), C_4 (120.63), C_5 (110.50), C_6 (120.94), C_7 (133.76), C_8 (126.25), and C_9 (123.27) ppm. These chemical shift values measured for the H and C atoms of the [Ag(indz)$_2$NO$_3$] complex are either very close to or have the same value as those of the free indazole molecule. According to these results, the complexation of the free ligand with AgNO$_3$ did not show an important shift in the experimental ^{1}H and ^{13}C NMR spectra. Many studies in the literature support our findings, and they all agree that this is generally true for Ag(I) complexes of *N*-donor ligands with relatively weak Ag-N and Ag-O interactions [59,60].

In a study conducted by Soliman et al. in 2018, [Ag$_2$L$_2$(NO$_3$)$_2$], a silver nitrate complex of a manlonamide-type ligand (L), was synthesized, and ^{1}H NMR spectrum assignments of both free and coordinated ligand were carried out. In this study, it was reported that the ^{1}H NMR chemical shifts were similar for the free ligand and the complex structure due to the relatively weak complexation of the Ag (I) atom with both the nitrate group O atom and the *N*-donor ligands [60]. Ag(2Cl-quinox)(NO$_3$)] and [Ag$_3$(2Cl-quinox)$_4$(NO3)$_3$] complexes of the 2-chloroquinoxaline ligand have been synthesized in the literature. In that study, ^{1}H NMR analyses of both the free ligand and the two synthesized complexes were performed. Some data from Ag(I) complexes showed the same shift as the free ligand, while others did not, according to the findings [59]. Another study evaluated the Ag(I) complex with isoniazid, an antimicrobial drug. When the spectrum of the ligand was compared with that of the metal complex, the most remarkable change was in the signals of the hydrogen atoms of the NH$_2$ group, while the others showed less significant shifts [64]. Another example of a study is the NMR analysis of the [RuCl$_3$(H$_2$O)(Hind)$_2$] complex of indazole. The same signal sets were observed in the ^{1}H NMR spectra for both the metal-free indazole and the coordinated indazoles with the same multiplicity [65]. Also, there are no significant differences between the experimental and calculated chemical shift values of both the ligand and the complex.

3.4. UV–Vis spectral analysis

The experimental and calculated wavelengths, excitation energy, oscillator strength, and major contribution are listed in Table 1. A broad absorption band for the free indazole ligand was determined at 299 nm. The experimental spectrum of the [Ag(indz)$_2$NO$_3$] complex shows 3 absorption bands at 299, 286 and 260 nm in Fig. 2. From the theoretical calculations, the absorption peak was found at 251 nm, resulting from the Homo-4/Lumo + 1 and Homo-4/Lumo transitions, and it is quite compatible with the experimental values at 260 nm. When the experimental UV–Vis spectra of the free ligand and the complex were compared, the formation of new absorbance peaks in the spectrum of the [Ag(indz)$_2$NO$_3$] complex and the wavelength shifts after complexation supported the coordination of the free ligand with the Ag(I) ion.

3.5. Mass spectrometry

Mass spectrometry is the most important structural characterization technique used in coordination chemistry to elucidate the main molecular ion peaks of synthesized complexes. The mass spectrum of the complex presenting fragmented ion peaks in the x-axis and *m/z* value is given in Fig. 3. The mass spectrum shows the molecular peaks at 224.9651 (15%) for $[AgC_7H_6N_2]^+$, 265.9923 (10%) for $[AgC_7H_6N_2(H_2O) + Na]^+$, 343.0184 (10%) for $[AgC_{14}H_{12}N_4]^+$, and 465,0517 (10%) for $[AgC_{14}H_{12}N_4(H_2O)_2 + Na + NO3 + H]^+$.

Table 1
Experimental and calculated UV–Vis wavelength (λ), excitation energy (eV) and oscillator strength for the [Ag(indz)$_2$NO$_3$] complex.

Experimental	Theoretical				
λmax (nm)	λmax (nm)	E (eV)	f	Symmetry	Major Contributions
260	251	4.9445	250.75	Singlet-A	HOMO-4 LUMO + 1 HOMO-4 LUMO

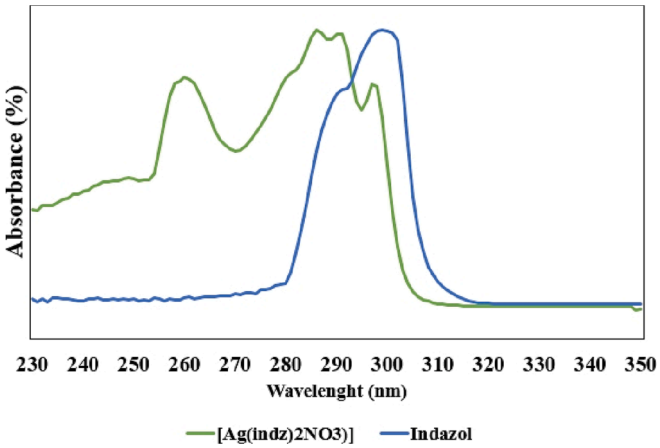

Fig. 2. Experimental UV–Vis spectra of indazole ligand and [Ag(indz)$_2$NO$_3$] complex.

3.6. Global molecular reactivity descriptor

The tendency of a molecule to donate and receive electrons is determined by the energy values of the highest-energy occupied molecular orbital (HOMO) and the lowest-energy unoccupied molecular orbital (LUMO) by electrons [66,67]. The energy difference between these molecular orbitals has an important role in the electronic, optical luminescence, photochemical reaction, UV–Vis, and even biological activity of a free ligand or metal complex [68–70]. If the energy values of the HOMO-LUMO orbitals are known, the ionization potential (I), electron affinity (A), global hardness (η), electronegativity (χ), chemical potential (μ_c), global softness (σ), and global electrophilicity (ω) values can be calculated with the equations below [67]:

$$I = -E_{HOMO} \quad (3)$$

$$A = -E_{LUMO} \quad (4)$$

$$\eta = (-E_{HOMO} + E_{LUMO})/2 \quad (5)$$

$$\mu_c = (E_{HOMO} + E_{LUMO})/2\mu \quad (6)$$

$$\chi = -\mu_c \quad (7)$$

$$\sigma = 1/\eta \quad (8)$$

$$\omega = (\mu_c^2)/2\eta \quad (9)$$

Table 2 shows the energy values of the quantum chemical properties of the indazole molecule and the [Ag(indz)$_2$NO$_3$] complex. Calculations for the free ligand were carried out using the 6–311++G(d,p) basis set, while the calculations for the complex structure were performed using the 6–311++G(d,p) and LanLDZ basis sets together. Calculated high HOMO energy values indicate that the molecule tends to donate electrons to the appropriate acceptor molecules with a low-energy empty molecular orbital. The lower value of LUMO energy suggests the molecule easily accepts electrons from the donor molecules. The E_{HOMO} and E_{LUMO} energies, indicating the ease of electron donation and electron acceptance between the substrate and target proteins, were found to be −6.36 and −1.19 eV for free ligand and −6.158 and −1.876 eV for the

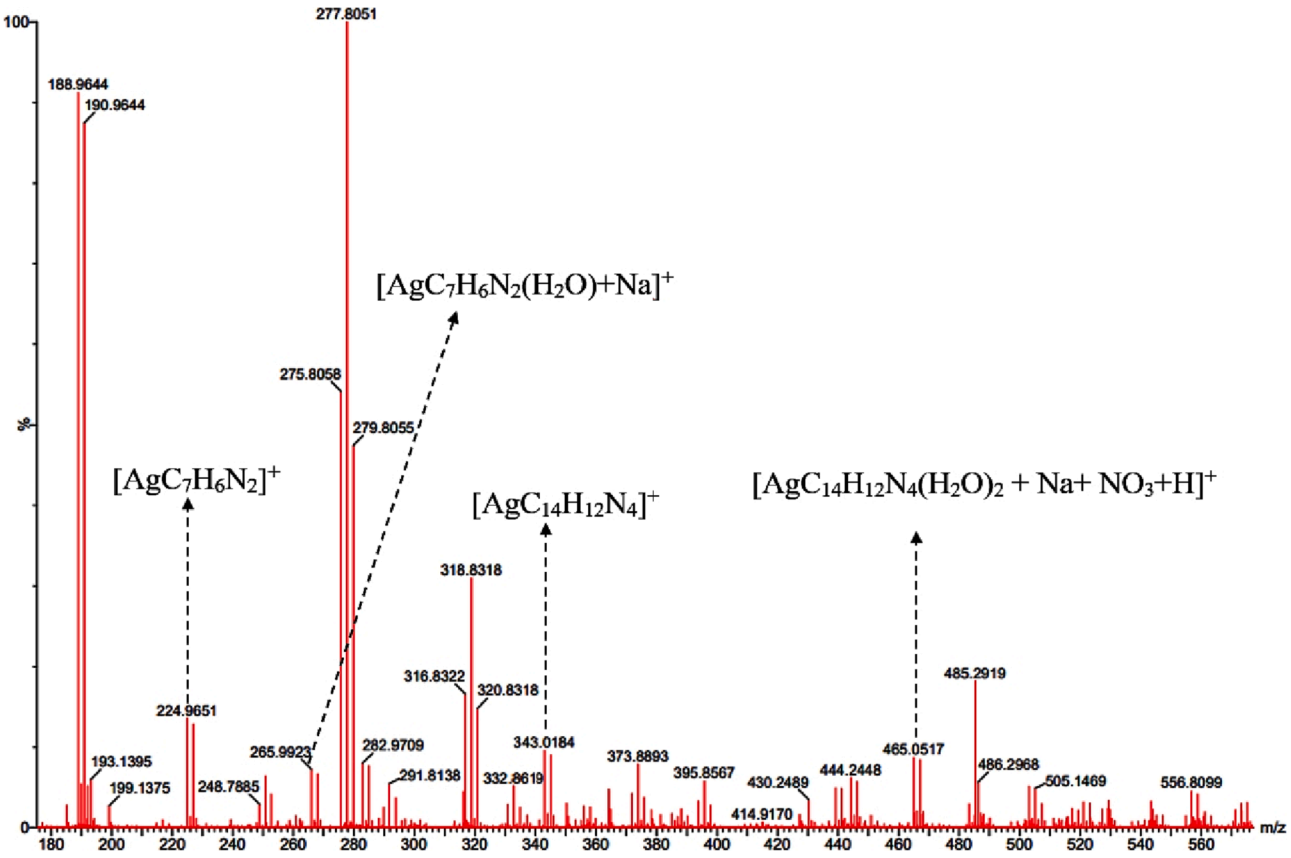

Fig 3. The mass spectrum of the [Ag(indz)$_2$NO$_3$] complex.

silver nitrate complex. As a result of the calculations, title compounds have the highest HOMO level and the lowest LUMO level, and these compounds appear to have the ability to donate electrons. The energy gaps (Eg) between LUMO and HOMO were calculated as 5.17 and 4.28 eV, respectively. The LUMO value of the synthesized complex structure is more negative and the HOMO value is more positive than that of the free ligand, and as a result, the HOMO-LUMO energy gap of the complex structure was found to be smaller. That is, the binding of silver nitrate to the free ligand increased its reactivity. Also, the η and σ values for the indazole molecule were determined as 2.58 and 0.38 eV, while these parameters were found to be 2.14 and 0.47 eV for the complex. According to ΔE, η, and σ values, both the indazole molecule and the [Ag(indz)$_2$NO$_3$] complex have low reactivity and tend to be chemically stable. In addition, there are many studies in the literature on different structures that support the obtained results [67,71,72]. The HOMO-LUMO distributions of both the indazole molecule and the title complex were given in Fig. 4. The HOMO and LUMO distributions for the indazole molecule are over almost the entire molecule. HOMO was distributed over the silver atom and nitrate group in the Ag(I) complex of indazole, while LUMO was distributed over the ligand on the left.

3.7. Molecular electrostatic potential (MEP) map analysis

The MEP map is one of the important analyses used to predict electrophilic (negative potential) and nucleophilic (positive potential) regions of organic or inorganic molecules. That is, it is a pretty good estimator for estimating charge density [73]. It also provides information on chemical reactions, hydrogen bond interactions and biological activity prediction. The electrostatic potential magnitude is defined by a color scale as follows: red < orange < yellow < green < cyan < blue [74]. The red, yellow, green, and blue in this color scheme indicate negative, slightly electron-rich, zero potential, and positive regions, respectively [75]. Fig. 4 presents 3D MEP maps prepared for the indazole molecule and [Ag(indz)$_2$NO$_3$] complex. When the MEP map of the indazole molecule is examined, it is seen that the N_2 atom is in the red (negative/electrophilic) region. In addition, all the C atoms in the benzene and pyrazole rings and the N_1 atoms of the indazole molecule are in the yellow (slightly electron-rich) region, while all the H atoms are in the positive, that is, blue-colored region. According to the MEP map of the complex structure, the negative region is concentrated on the O atoms of the nitrate group. When the free indazole molecule formed a compound with silver nitrate, the C and N atoms in its rings had a more positive value than in the free state. That is, the electron density is shifted on the O atoms. Similar results were obtained in previous studies on silver nitrate complexes in the literature [37,61].

3.8. Fukui functions

Fukui functions give information about the tendency of organic or inorganic molecules to lose and gain electrons. That is, it is used to determine electrophilic and nucleophilic atom sites in molecules. In other words, it indicates which atom is more susceptible to an electrophilic or nucleophilic attack [76]. Fukui functions are defined with the following equations for the neutral, cationic, and anionic states of the molecule using finite difference methodology:

$$f_k^- = q_k(N) - q_k(N-1) \quad (10)$$

$$f_k^+ = q_k(N+1) - q_k(N) \quad (11)$$

$$f_k^0 = (1/2)[q_k(N+1) - q_k(N-1)] \quad (12)$$

$f_k^+ f_k^- f_k^0$ In these equations and are defined as nucleophilic and electrophilic attack indexes according to the electron loss and gain status of a molecule, respectively. is also the neutral attack index [77]. The

Table 2
The calculated HOMO-LUMO energy gaps and quantum chemical propertiys values of the indazole molecule and the [Ag(indz)$_2$NO$_3$] complex.

Molecular Orbitals	Energy (eV)			Energy gap (eV)		Ionization potential (I) (eV)		Electron affinity (A) (eV)		Global hardness (η) (eV)		Electronegativity (χ) (eV)		Chemical potential (μ_c) (eV)		Global softness (σ) $(eV)^{-1}$		Global electrophilicity (ω) (eV)	
	*	**		*	**	*	**	*	**	*	**	*	**	*	**	*	**	*	**
H	−6.36	−6.16	ΔE_{H-L}	5.17	4.28	6.36	6.16	1.19	1.87	2.58	2.14	3.77	4.01	−3.77	−4.01	0.38	0.46	2.75	3.76
L	−1.19	−1.87																	
H-1	−6.90	−6.63	$\Delta E_{H-1-L+1}$	6.60	5.03	6.90	6.63	0.29	1.60	3.30	2.51	3.59	4.11	−3.59	−4.11	0.30	0.39	1.96	3.36
L + 1	−0.30	−1.60																	
H-2	−8.27	−6.96	$\Delta E_{H-2-L+2}$	8.24	5.83	8.27	6.96	0.03	1.13	4.12	2.91	4.14	4.04	−4.14	−4.04	0.24	0.34	2.08	2.80
L + 2	−0.03	−1.13																	

H: HOMO (Highest Occupied Molecular Orbital), L: LUMO (Lowest Unoccupied molecular orbital), eV: electron volt, $(eV)^{-1}$: 1/electron volt.
*Energy values for indazole molecule.
**Energy values for [Ag(indz)$_2$NO$_3$) complex.

electron population in the r[th] atom is represented by qk, and the charge amounts of the molecule in the neutral, anionic, and cationic states are q_kN, q_k(N + 1), and q_k(N-1). In order to provide a clear distinction between nucleophilic and electrophilic regions, Δf(r) which is a new dual descriptor, is used and calculated by the following equation [78].

$$\Delta f(r) = f^{+}(r) - f^{-}(r) \tag{13}$$

When Δf(r) > 0, the region is electrophilic (is favored for a nucleophilic attack), and when Δf(r) < 0 the region is nucleophilic (is favored for an electrophilic attack) [79]. The Fukui function values for the indazole molecule and the [Ag(indz)$_2$NO$_3$] complex are presented in supplementary Table S5. Also, graphical representations of the dual descriptors of the indazole molecule and [Ag(indz)$_2$NO$_3$] complex are presented in supplementary Fig. S5 [80].

The blue and green colors indicate negative and positive sites, respectively, in the dual descriptor Fukui function images [79]. The N_1, C_7, and C_9 atoms of the indazole molecule are in the blue-colored region. Therefore, these atoms are located in the electrophilic region. The dual descriptor image of the indazole molecule is also consistent with the results calculated with the Gaussian 09 program and given in supplementary Table S5. According to the image created for the [Ag(indz)$_2$NO$_3$] complex, the N_1, C_9, N_{16}, Ag_{31}, O_{33}, O_{34}, and N_{35} atoms are located in the blue-colored (electrophilic) region, and this image is quite in harmony with the results presented in supplementary Table S5.

3.9. Charge analyses

NBO, Hirshfeld, and APT charges were calculated to investigate the bonding ability of the atoms of the indazole molecule and the [Ag(indz)$_2$NO$_3$] complex. The 6–311++G(d,p) basis set was used in the calculations for the free ligand, while the 6–311++G(d,p) and LanL2DZ basis sets were used together in the complex structure calculations. With these charge analysis calculations, the electronic charges and binding potentials of atoms were explained [81]. The calculated charge values are listed in supplementary Table S6 and are presented graphically in supplementary Fig. S6 for both the indazole molecule and the Ag(I) complex.

According to APT, NBO, and Hirshfeld charge analyses, N_1, N_2, C_4, C_5, and C_9 atoms have a negative value, while C_3 and all H atoms have a positive value. These results are also similar to the results obtained from the MEP map. Similarly, N_1 and C_9 atoms have also been found to be in the electrophilic region in Fukui function analyses. According to the results of all three charge analyses of the Ag(I) complex structure, all C atoms except for C_3, C_7, C_{18}, and C_{23} atoms, N_1, N_2, N_{16}, N_{17}, O_{32}, O_{33}, and O_{34} atoms have negative values, and Ag_{31}, N_{35}, and all H atoms are also found to have positive values. The results obtained from the charge analyses for the complex structure are also similar to those obtained from both the MEP map and the Fukui functions. The most negative atom for the indazole molecule is N_1. As a result of the complexing of the indazole molecule with silver nitrate, the N_1 atom has a less negative value, while the atoms with the highest negative values are the O_{33} and O_{34} atoms in the nitrate group. These results are also similar to those obtained from the MEP map.

3.10. AIM and NCI-RDG calculations

The atoms in molecules (AIM) and non-covalent interactions (NCI) were calculated to investigate the intramolecular and intermolecular interactions between the Ag(I) cation and the indazole molecule. The QTAIM method, when applied to the complex system, identifies the bond paths between specific atoms and the corresponding BCPs, or critical points of chemical bonds, in the electron density distribution. Around the Ag atom, there are four close neighbors. The metal center is coordinated by two nitrogen atoms and two oxygen atoms among these neighbors.

Graphical representations of the AIM analysis of the Ag(I) complex

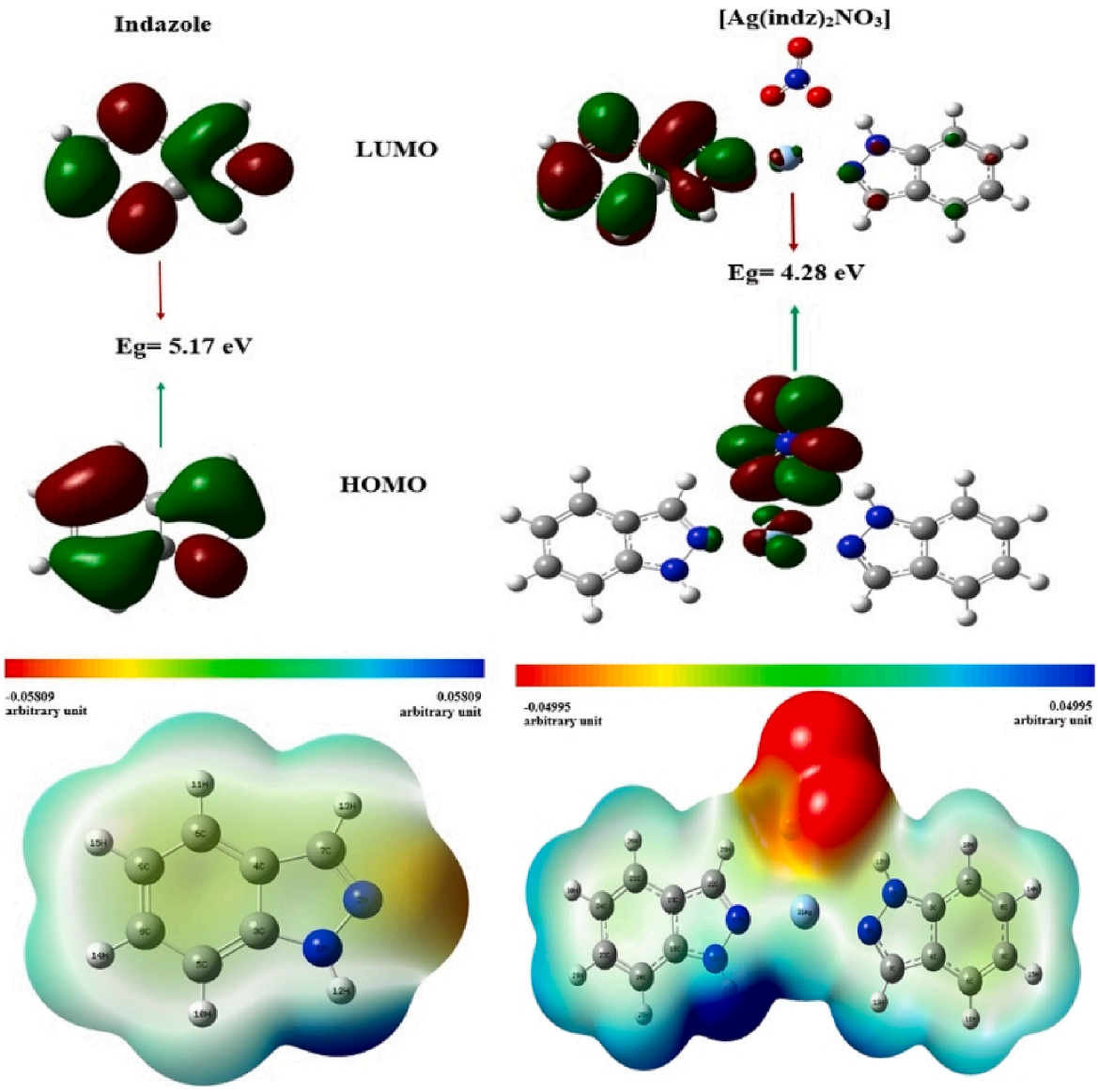

Fig. 4. FMO diagrams and MEP maps of the indazole molecule and the [Ag(indz)2NO3] complex.

are shown in supplementary Fig. S7 using Multiwfn. R. Bader [32,33,82,83] has developed the innovative approach AIM [84], which proposes that the electron density ρ(r) is a local function of the molecular system. This approach is widely used to determine inter- and intra-atomic interaction calculations. The topological parameters, which are the electron density ρ(r), the Laplacian, $\nabla^2\rho(r)$ the kinetic energy densities G(r), the total energy densities H(r), the potential V(r), and the bond energy E give a lot of information on the properties of BCPs and CPs. Hence, the different topological properties of the title complex are collected in detail in Table 3. According to Rozas et al. [85], these hydrogen bonds are strong hydrogen bonds if the electron density is $\nabla^2\rho(r) < 0$, and the total energy density is H (r) < 0. If $\nabla^2\rho(r) > 0$, H(r) > 0 it is considered a weak hydrogen bond. According to the results, the Laplacian of charge density values are positive, indicating that the electronic charge is depleted along the binding pathway and the presence of ionic interaction [86]. The AIM results showed that the Ag(I) complex is characterized by BCPs, which define the BCPs are located at O… H links, these bonds with the energy densities of C—H…O and N—H…O are weak and medium hydrogen bonding, respectively. As seen from Table 3 indicates that in the intramolecular contacts N—H…. O in complex has the highest value of interaction energy, so it is the strongest interaction. Jenkins and Morrison [87], and Espinosa [88]

Table 3
Topological parameters (in a.u) obtained by QTAIM analysis for Ag(I) complex.

Interactions	ρ(r)	$\nabla^2\rho(r)$	H(r)	G(r)	V(r)	E_{bond}(kJ/mol)	|V(r)|/ G(r)	λ_1	λ_2	λ_3
Ag-N_{17}	0.06511	0.28922	−0.0011	0.08248	−0.09266	121.63	1.1234	−0.07415	−0.07024	0.43362
Ag-N_2	0.06688	0.29444	−0.0109	0.08455	−0.09550	125.36	1.1295	−0.07651	−0.07247	0.44343
Ag….O_{32}	0.02223	0.08571	0.00067	0.02082	−0.02021	26.53	0.9707	−0.01820	−0.01745	0.12137
Ag….O_{33}	0.03280	0.14712	0.00053	0.03624	−0.03571	46.87	0.9853	−0.03295	−0.03063	0.21071
C_{22}-H_{28}….O_{33}	0.01182	0.04301	0.00167	0.00907	−0.00739	9.70	0.8147	−0.01214	−0.01014	0.06529
N_1-H_{12}….O_{32}	0.03551	0.12728	0.00038	0.03143	−0.03105	40.76	0.9879	−0.05537	−0.05130	0.23396

et al. proposed that bond interactions are sorted according to the |V(r)|/G(r) ratio. In the ratio |V(r)|/G(r) < 1, the bonded interaction is regarded as the closed shell, when |V(r)|/G(r) > 2, it is considered as the typically covalent interaction, and when 1 < |V(r)|/G(r) < 2, it is the intermediate character. The mean |V(r)|/G(r) ratio for the H···O interactions is<1.0, as shown result, these interactions are mostly the closed shell for the complex model. The CPs of Ag-N interactions constitute the covalent character ($\nabla^2\rho(r) > 0$ and H(r) < 0) bonds in the optimized geometry of the title complex. Moreover, the metal ion and oxygen (Ag…O) interactions have a covalent character of the bonds.

The reduced density gradient (RDG) shows intra- and inter nonbonded interactions in a chemical system [89]. Fig. S7 displays the RDG scatter graph, which displays the various regions through spikes. As can be seen, these interactions are indicated by regions that are colored blue, red, and green, which correspond to the stabilization of H-bonds, the destabilization of steric interactions, and van der Waal's interactions, respectively. There is a light blue dot, which shows that there are strong attractive interactions N_1-H_{12}….O_{32}. The red elliptical plate in the center of the pyrazole and benzene rings describes the destabilizing steric interaction, and the green plates represent the regions of weak interaction C_{22}-H_{28}…….O_{33}, which are attributed to the VDW interactions. These results are in line with what the AIM study and the assessment of atomic charges found.

3.11. ELF and LOL analaysis

Electron localization function analysis (ELF) and localized orbital locator (LOL) analyses based on covalent bonding were performed with the Multiwfn program to reveal the regions where the probability of electron pairs on the molecular surface is high [90]. While ELF is an analysis method based on electron pair density, LOL is usually observed when localized orbitals overlap. But both analysis methods have similar chemical content and give results depending on kinetic energy density. The ELF isosurface 2D maps plotted in the range of 0.0–1.0 for free ligand and complex structure are presented in Fig. 5. In this map, the range of 0.5–1.0 indicates the presence of bonding and nonbonding localized electrons, while the range of 0.0–0.5 indicates the presence of delocalized electrons [66,90].

For both molecules, the red color on the H atoms represents a strong electronic localization. Also, the blue color around the C, N, and Ag atoms represents a depletion region between the inner shell and the valence shell, that is, it indicates the delocalized electron density. Similarly, values>0.5 in LOL maps also indicate high localization of electrons due to the presence of a nuclear shell [91].

3.12. Nonlinear optical properties

Because of the growing interest in non-linear organic and inorganic materials' technical applications, the electric dipole moment, average polarizability, anisotropy of polarizability, and first hyperpolarizability values for the indazole molecule and Ag(I) complex structures were calculated in this section of the study [79,92]. The results are listed in supplementary Table S7. While the dipole moment value of the indazole moment was calculated at 1.84 Debye, this value was found to be 9.62 Debye for the [$Ag(indz)_2NO_3$] complex. The initial polarizability values of the free ligand and complex were found to be 1.48×10^{-30} and 5.08×10^{-30} esu, respectively. When these two values are compared to the value of urea, which is used as the brink value in determining a structure's nonlinear properties, the indazole molecule has a value that is approximately 4 times higher, and the Ag(I) complex has a value that is approximately 14 times higher [93,94]. According to these results obtained from theoretical calculations, while the free indazole molecule has moderate non-linear optical properties, its complex formation with silver nitrate increased its non-linear optical properties. Therefore, we can say that the complex structure has very good non-linear properties.

3.13. Thermodynamic properties

The thermodynamic parameters of a compound can explain its stability and reactivity. The supplementary Table S8 lists the thermodynamical parameters such as entropy (S), enthalpy (H), zero-point vibration energy (ZPVE), Gibbs free energy (G), and geat capacity (Cp) of the free ligand and its Ag(I) complex in the gas phase at various temperatures ranging from 100 to 1000 K using the B3LYP/6–311++G (d,p) basic set. These theoretical results are helpful in estimating the chemical reaction direction. The thermodynamic function also increased linearly as the temperature increased from 100 to 1000 Kelvin, as shown in Table S8. This linear variation indicates that the vibrational intensities of molecules increase with temperature [95].

In Table S8, the enthalpy is calculated as a function of temperature. When compared to free indazole structures, the Ag(I) complex has an almost exponential behavior as the temperature rises, a higher intensity level, and its energy is less likely to be removed as heat. Furthermore, it was found that as the temperature increased, the entropy of the complex structure was higher than that of the free ligand. For both of the structures under consideration, we see that as temperature rises, enthalpy and entropy both rise while Gibbs free energy falls. All of these reactions are endothermic in this way. Additionally, we see that the indazole structure has a significantly lower free energy than the complex structure.

3.14. Thermal analysis (DSC-TGA) of the metal complex

Thermal properties such as thermal behavior, thermal stability, and thermiogravimetric analysis for compounds are identified using the DSC-TGA method [96]. Supplementary Fig. S8 depicts the differential scanning calorimetry (DSC) curve for measuring temperature differences and the thermogravimetric analysis (TGA) curve for measuring sample weight loss. The TGA curve illustrates that the Ag(I) complex thermally decomposes in four steps that follow one another in supplementary Fig. S8. The TGA curve stands for a couple of steps in the mass loss, with the main mass loss of 37.71% placed between 650 and 700 °C. The first step occurs in the temperature interval from 150 to 200 °C with an experimental mass loss of 18.1% corresponding to the decomposition of the nitrate anions. The second step occurs in the temperature interval from 250 to 300 °C with a mass loss of 20.8% corresponding to the decomposition of indazole ligand molecules. In the final step, the remainder of the complex, representing 11.7% of its mass, was decomposed. The DSC curves appear sharp, which suggests that the material is highly pure, that there was no phase transition prior to melting, and further, that the compound is fragmented gradually [97]. In the thermal decomposition of the complex, an exothermic process (at 117.6 °C) and two endothermic processes (at 189.2 °C and 234.2 °C) are also represented by the DSC curve (see Fig. S8).

4. Biological activities

4.1. Antioxidant activity (DPPH• free radical scavenging activity)

The DPPH method was used to assess the antioxidant activity of indazole and its Ag(I) complex in vitro. To compare the results, ascorbic acid and BHT were used as the standard antioxidants. One of the most widely used spectrophotometric methods for measuring antioxidant activity is the DPPH method [98]. An illustration of the inhibition study is shown in Fig. 6.

Table 4 and Fig. 7 show the results.

The antioxidant activity of the free ligand indazole and silver complex at low concentrations (100 μg/ml) was compared. The percent DPPH radical inhibition of ligand, complex, and standards (ascorbic acid and BHT) at 0 min, 30 min, 3 h, and 24 h was calculated. After 30 min, the percent inhibition values of all samples decreased. Therefore, all comparisons were made according to the 30th minute. Indazole ligand

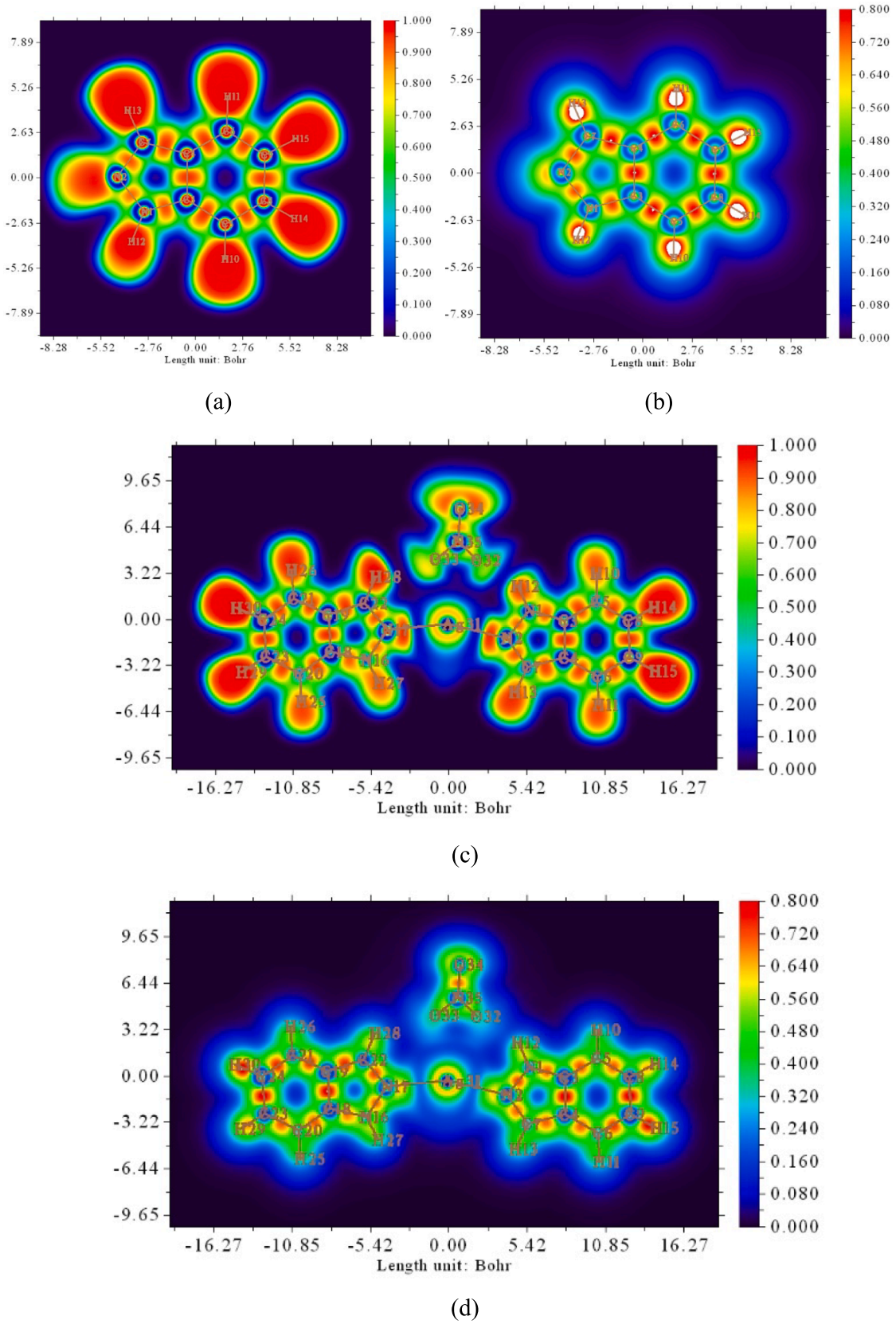

Fig. 5. ELF (a,c) and LOL (b,d) map of indazole molecule and $[Ag(indz)_2NO_3]$ complex.

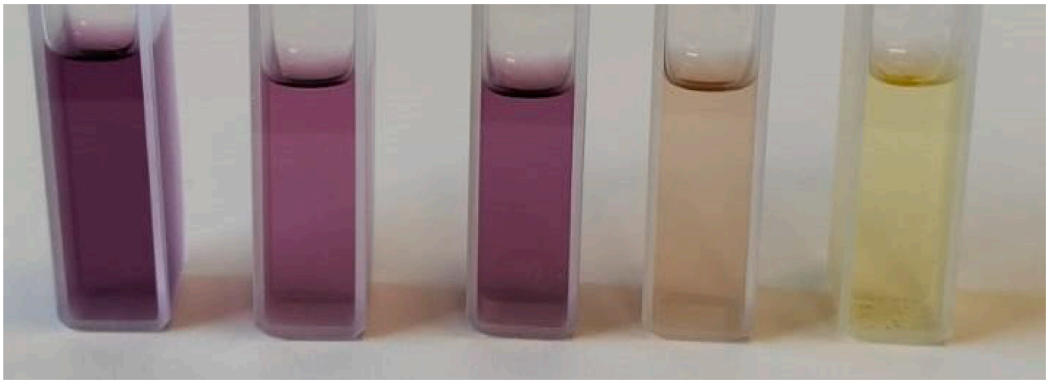

Fig. 6. A (Control), B (Indazole), C (Indazole-Ag complex), D (standart BHT), E (standart Ascorbic acid).

Table 4
% DPPH free radical inhibition of samples*.

Compound	0 min	30 min	3 h	24 h
Indazole (Free ligand)	48.32 ± 1.29	52.11 ± 1.41	49.95 ± 1.22	47.11 ± 1.59
Ag(I) complex	39.29 ± 1.34	43.82 ± 1.63	40.95 ± 1.38	37.98 ± 1.65
Standard (BHT)	70.12 ± 1.86	76.82 ± 1.34	72.85 ± 1.24	66.93 ± 1.57
Standard (Ascorbic acid)	81.68 ± 2.23	84.11 ± 2.65	82.21 ± 1.86	79.45 ± 1.43

*Again, numbers (n = 3) were analyzed for each group examined in this study. The study's results are given as the mean ± standard deviation.

was found to have higher percentages of inhibition values than its Ag(I) complex. The DPPH radical scavenging activities of the samples were determined in this study as ascorbic acid > BHT > free ligand > Ag(I) complex.

There is a relationship between DPPH percentage and antioxidant capacity. The higher the inhibition percentage, the higher the antioxidant capacity. However, the IC_{50} value is defined as the amount of an antioxidant substance required to reduce 50% of the initial DPPH concentration [99,100]. In other words, lower IC_{50} values indicate higher anti-radical activity. In addition, the IC_{50} values of the samples at 30th minutes were calculated in this study. In this study, inhibition percentages and IC_{50} values of the free ligand and silver complex were calculated. For this purpose, solutions were prepared from indazole, [Ag$(indz)_2NO_3$] complex, and standard substances (BHT and ascorbic acid) at 25, 50, and 100 μg/mL concentrations. The percent inhibition values of each sample against three different concentrations were calculated. Graphs with % inhibition values versus concentrations were drawn. The IC_{50} values of each sample were calculated from the correct equation of the graphs. The IC_{50} values of indazole and [Ag$(indz)_2NO_3$] complex were compared with the IC_{50} values of standard (BHT, ascorbic acid) substances. As a result, it was determined that ascorbic acid (11.22 μg/mL) > BHT (23.91 μg/mL) > indazole (90.97 μg/mL) > Ag(I) complex (117.57 μg/mL). In a study, the antioxidant capacity of coordination compounds formed by 4,5,6,7-tetrahydro-1H-indazole with Cu (II), Co (II), and Ag (I) was investigated by the DPPH method. The 4,5,6,7-tetrahydro-1H-indazole-Ag complex has a % inhibition value of 57.89 and an IC_{50} value of 82 μg/mL at 125 μg/mL concentration [101]. In a study, total antioxidant capacity analyses of tetrahydroindazoles and their derivatives were performed, and the percent inhibition and IC_{50} values of these substances were calculated. It has been reported that the percentages of inhibition of these substances at 100 concentrations ranged from 13.51 ± 1.5 to 47.72 ± 4.4. In addition, it was determined that the IC_{50} values of these substances were > 100 [79]. The IC_{50} values of 7-carbo-substituted 5-bromo-3-methylindazoles and their derivatives were calculated and reported to vary between 0.91 ± 0.004 and 88.66 ± 0.001 μM [102]. Our findings were found to be compatible with the literature.

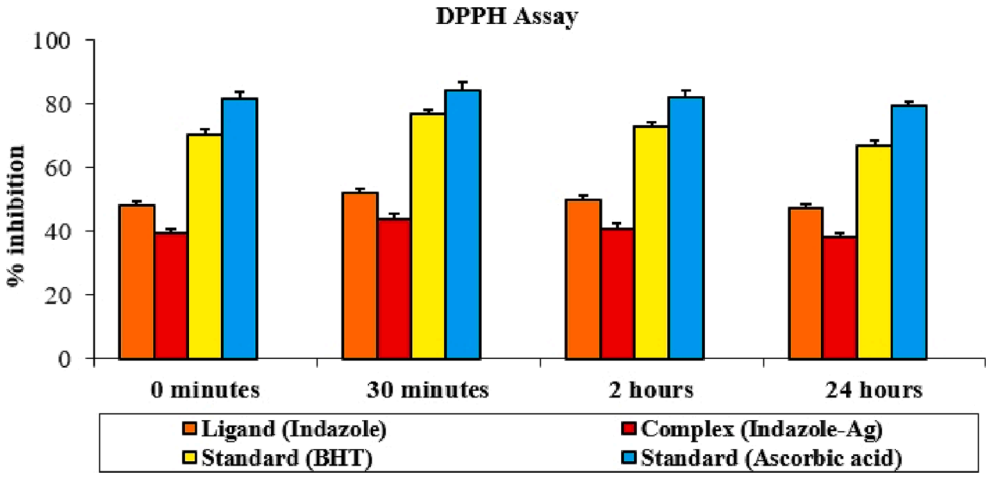

Fig. 7. Percentage of DPPH radical inhibition in samples (100 μg/mL).

4.2. Antimicrobial study

Four gram-positive bacteria (*S. aureus, B. cereus, E. faecalis, and B. subtilis), five gram-negative bacteria (P. aeruginosa, V. anguillarum, K. pneumoniae, E. coli*, and *A. hydrophila*), and a yeast strain (*C. albicans*) showed the particular antimicrobial activity of the Ag(I) complex. Table 5 presents the findings. In the control, there was no inhibition zone (DMSO). In this investigation, the metal complex showed strong antimicrobial activity against the microorganisms tested. The antimicrobial activity of the Ag(I) complex was nearly identical to that of the widely used medication tetracycline.

Ag(I) complex, *S. aureus* (DIZ:30 mm and MIC: 8 mg/ml), *B. cereus* (DIZ: 28 mm, MIC 16 mg/ml), *P. aeruginosa* (DIZ: 26 mm, MIC: 8 mg/ml), *V. anguillarum* (DIZ: 25 mm, MIC: 8 mg/ml), *K. pneumoniae* (DIZ: 22 mm, MIC: 8 mg/ml) and *C. albicans* (DIZ: 25 mm, MIC: 8 mg/ml) against exhibited strong antimicrobial activity.

The Ag(I) complex was identified as the most effective enhancer of antimicrobial activity against *S. aureus* in the test set. Silver ions cling to the proteins in bacterial cell membranes, enter cells, and bind to DNA to stop cell division. Additionally, silver ions stop the bacterial respiratory system and kill the cell's ability to produce energy. At some point, the bacterial cell membrane ruptures, killing the bacteria [103].

Microbiological resistance to antiseptics is a hotly debated subject as a result of the increased attention being paid to bacterial resistance to antibiotics. Compared to antibiotics, topical antiseptics like silver have a lower chance of bacterial resistance because they have several antimicrobial sites of action on their target cells. According to reports, the danger of resistant pathogens to silver in wound healing is low, and silver-containing creams remain an extremely important tool in wound infection management [104,105].

As a result of tested free ligand biological studies, diameter of inhibition zone (DIZ, mm) and minimum inhibitory concentration (MIC, μg/ml), (DIZ: 17 mm, MIC: 16 μg/ml), (DIZ: 12 mm, MIC: 16 μg/ml) and (DIZ: 18 mm, MIC: 16 μg/ml) were found to show good activity against *S. aureus, B. cereus* and *C. albicans*, respectively. The free ligand was compared with standard tetracycline and natamycin. The inhibition zone and MIC values for the substances that were examined are shown in Table 5 below.

4.2.1. Testing for QSI action of indazole and its Ag(I) complex

By inhibiting the growth of the violacein pigment to a diameter of 26 mm and 16 mm after 24 h at 28 °C, the Ag(I) complex and free ligand demonstrated a significant QSI action against *C. violaceum* ATCC 12472. (Table 5). According to the strong quorum sensing inhibition (QSI) value, the $[Ag(indz)_2NO_3]$ complex can fight infection pathogenesis and spread via QSI. Whereas free ligand showed a more moderate inhibition of quorum sensing inhibition (16 mm).

4.3. Docking results

In-silico molecular docking studies aid in predicting the probable binding mode and mechanism of action of bioactive chemical constituents against metabolic key proteins [106]. The results of in-vitro antioxidant and antibacterial activities were used to calculate molecular docking in order to obtain a more accurate description of the inhibitory capability of the compound and to establish a correlation between these activities. In our study, we investigated how the title compounds, which are a component of the structure of many biologically active compounds containing the indazole ring system [107,108], are docked against antioxidant enzymes and antibacterial proteins. While examining ligand-enzyme interactions, which play a critical role in drug design and discovery, two microbial pathogen proteins (*S. aureus and C. albicans*), which show the highest activity according to their in vitro antimicrobial results, were selected and examined. Also, the antioxidant potential exhibited by performing docking studies with the receptors Peroxiredoxin (3MNG) is a well-known human antioxidant enzyme that consists of an electron donor and a catalyst species, i.e., thioredoxin and essential cysteine residues, respectively. These species contribute to the cellular metabolic response to reactive oxygen species and assist in peroxide scavenging [109]. The result parameters of the docking study related to the antioxidant and antimicrobial potential exhibited by the free indazole ligand and its Ag(I) complex are presented in Table 6. The 2D representation of the investigated ligand-receptor interaction and the 3D representation are given in Fig. 7. According to the free binding energy values in Table 6, these complexes bind to their respective enzyme targets reasonably. The stronger the binding affinity between complex molecules and receptor proteins, the more stable the ligand-enzyme complexes form [110]. Ag(I) complexed with *S. aureus* (5FPO) has a binding energy of -8.43 kcal.mol^{-1} and *C.albicans* (4LEB) has a binding energy of -6.67 kcal.mol^{-1}, whereas the free ligand has binding energies of -5.60 and -4.67 kcal.mol^{-1}. In this case, the metal complex showed stronger inhibitory activity compared to the free ligand. The docking study results were found to be in good agreement with the in vitro antimicrobial results and to follow the antimicrobial activity order

Table 5
Antimicrobial properties of the medication reference and the Indazole and ıts Ag(I) complex against the examined bacteria.

Compounds							
	Indazole		**$[Ag(indz)_2NO_3]$**				
Organisms	**DIZ (mm)**	**MIC (μg/ml)**	**DIZ mm)**	**MIC (μg/ml)**	**Tetracycline (10 mg/ml)**	**DMSO**	**$AgNO_3$**
Gram (+)							
S. aureus (ATCC 25923)	17	16	30	8	23	–	10
B. cereus(709 Roma)	12	16	28	8	26	–	10
B. subtilis (ATCC6633)	10	512	12	128	25	–	8
E. faecalis (ATCC29212)	–	–	16	16	24	–	5
Gram (-)							
E. coli (ATCC 25922)	–	–	15	32	21	–	8
A. hydrophila (ATCC7966)	–	–	12	64	22	–	5
P. aeruginosa (ATCC 27853)	–	–	26	8	21	–	8
V. anguillarum (ATCC 43312)	–	–	25	8	20	–	8
K. pneumoniae (ATCC 13883)	10	256	22	16	23	–	10
Yeast					**Natamycin (30 mg/ml)**		
C. albicans (ATCC 90028)	18	16	25	8	24	–	10
Anti-quorum sensing activity							
C. violaceum (ATCC 12472)	16	32	26	8	–	–	8

Notes: Inhibition zones include diameter of hole (6 mm). Sample amount 50 μl. _, not active. **DIZ:** Diameter Inhibition Zone, **MIC:** Minimum Inhibitory Concentration, **DMSO:** Dimetil sülfoksit.

Table 6
Docking parameters of title compound docked with the antioxidant and antimicrobial targets.

Protein (PDB ID)	Compound	H-Bonded residues	No of hydrogen bonds	Bonded distance (Å)	Hydrophobic interacting residues	Binding energy (kcal/mol)
3MNG	Free ligand	GLU 16	3	2.05	ARG 86, ALA 90, LEU 96	−4.83
		VAL 94		2.14		
		LEU 96		1.77		
	Ag(I) complex	LEU 96	5	2.61	GLU 16, ARG 95, LEU 96	−8.89
		GLU 16		2.06		
				1.83		
				2.84		
		GLY 92		2.37		
4LEB	Free ligand	PHE 60	2	2.02	THR 65, PHE 81	−4.67
				1.96		
	Ag(I) complex	LYS 59	2	2.95	PHE 81, PRO 29,	−6.67
		THR 62		2.03	THR 61,ALA 83,VAL 172	
5FPO	Free ligand	ILE 218	3	2.24	GLU 110, PHE 217, TYR 219, ASN 247	−5.60
		ASN 247		2.29		
		ARG 250		2.23		
	Ag(I) complex	LYS 112	3	2.12	LEU 80, LEU 82	−8.43
		ILE 113		1.93		
				1.70		

of the complexes. When the docking results for the antioxidant potential of the studied complexes were examined, it was understood that the active site inhibitory activity of the metal complexes was less than that of the free ligand (see Table 6). The binding energies of complexes and proteins are determined by hydrogen bonding, Van der Waals interactions, and electrostatic interactions [111]. When electrostatic and Van der Waals interactions are coupled, H-bonds form. The total internal and binding energy is significantly influenced by interactions that can be seen in 2D and 3D shapes. The group (-C═N-) is present in the investigated structures, which makes them active pharmacophores with excellent binding affinity for nucleophilic and electrophilic groups found in the active site of the enzyme and is the cause of their active nature for enzyme inhibitory activity [112]. In both compounds, nitrogen atoms of the pyrazole ring in all three receptors and amino acids intermolecular hydrogen bond H-bond interaction has occurred. As displayed in Fig. 8, indazole ligand was located in the antioxidant receptor 3MNG with the help of hydrogen bonds (GLU 16, VAL 94, LEU 96). Also, the Ag(I) complex represented three intermolecular hydrogen bonds between GLU16 (2.06,1.83, and 2.84 Å). Likewise, as shown in Fig. 8, the free ligand complexing with *C.albicans* exhibited two intermolecular hydrogen bond interactions between PHE 60 (2.02 Å and 1.96 Å). Similarly, the Ag(I) metal complex displayed two different

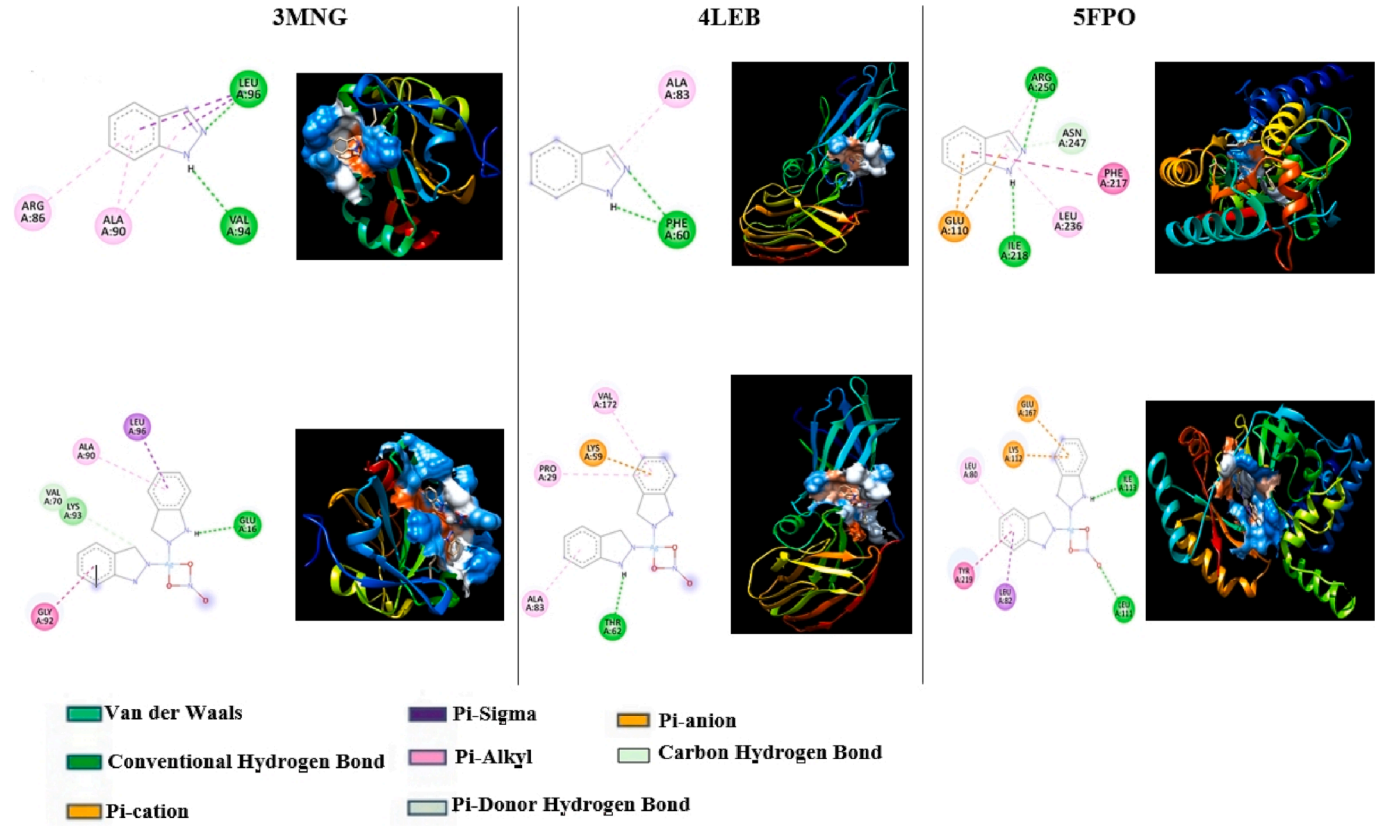

Fig. 8. 2D visual representations and 3D docking result representation of free ligand and its Ag(I) complex association with chosen targets.

intermolecular H-bonds between the pyrazole moiety's *N*-atom and LYS 59 (2.95 Å) and THR 62 (2.03 Å). Other analysis results show that the interactions have three π-Alkyl and one π-cation interactions with different active sites: PHE 81, PRO 29, ALA 83, VAL 172, and LYS 59 have bond lengths ranging from 3.05 to 3.56. The ligand and its metal complex have demonstrated significant interactions within the active sites of the *S. aureus* protein through key amino acids such as ASN 247. ILE 218, ARG 250, LYS 112, and ILE 113. All these interactions allow the stabilization of a ligand at the protein active sites. As a result of the findings, we can conclude that our compound has the potential to be an important antibacterial and antioxidant inhibitor.

5. Conclusion

The calculated characteristic vibrational modes of each grouping correspond to those observed in the experimental spectrum. The synthesized complex was characterized by ^{13}C and ^{1}H NMR, UV–Vis, and mass spectroscopy. The measurement of a linear optical parameter reveals that materials with low band gaps, which support the bioactivity of the molecule, are best suited for nonlinear optics. It has been detailed how there is a theoretical relationship between temperature and the thermodynamic functions, heat capacities, entropies, and enthalpies. Furthermore, the thermal stability of the synthesized Ag(I) complex was determined using TG/DSC analyses. According to QTAIM analysis, the Ag-N bonds have a covalent character, and the C—H…O and N—H…O hydrogen bonds are weak and moderate. According to the RDG analysis of non-covalent interactions, the complexes were stabilized by van der Waals interactions between the planes of the ligand molecules and bonds between the metal ions and the oxygen and especially nitrogen atoms. The discovery of new substances with effective and potent biological activities is one of the most important goals of pharmacological research today. Indazole and silver complexes showed DPPH radical scavenging activity even at low concentrations (100 μg/mL). It was also determined that indazole has a higher DPPH radical scavenging capacity than the silver complex. With this study, it was concluded that the ligand and its metal complex have moderate antioxidant capacity. According to the results of the biological activity tests, it was determined that while the free ligand showed good antimicrobial activity, the Ag(I) complex showed stronger antimicrobial properties. In this case, it is thought that the Ag(I) complex can be used as a building block in the synthesis of important new compounds that can be used as antimicrobial agents in the food and pharmaceutical industries. In molecular docking studies, the binding energies of the ligand and its metal complex to the active site of the enzymes were calculated. The results demonstrate that the Ag(I) complex is more active than the free ligand, indicating that better biotargets for the complexes are required.

6. Corresponding author declaration

The corresponding author of this manuscript, certifies that the contributors' and conflicts of interest statements included in this paper are correct and have been approved by all co-authors.

I further confirm that the manuscript has been read and approved by all named authors and that there are no other persons who satisfied the criteria for authorship but are not listed. We further confirm that the order of authors listed in the manuscript has been approved by all of us.

7. Author's countributions

All authors contributed to the study's conception and design. Material preparation, data collection, and analysis were performed by Ceyhun KUCUK, Senay YURDAKUL, Sibel Celik (synthesis, spectroscopic, and DFT calculations), Ebru Coteli (antioxidant activity), and Belgin ERDEM (antimicrobial activity). The first draft of the manuscript was written by Ceyhun KUCUK, and all authors commented on previous versions of the manuscript. All authors read and approved the final manuscript.

CRediT authorship contribution statement

Ceyhun Kucuk: Software. **Sibel Celik:** Conceptualization, Data curation, Methodology, Software, Supervision, Validation, Visualization, Writing – original draft. **Senay Yurdakul:** Conceptualization, Data curation, Investigation, Methodology, Software, Supervision, Validation, Visualization, Writing – original draft. **Ebru Coteli:** Writing – original draft. **Belgin Erdem:** Writing – original draft.

Declaration of Competing Interest

The authors declare that they have no known competing financial interests or personal relationships that could have appeared to influence the work reported in this paper.

Data availability

No data was used for the research described in the article.

Appendix A. Supplementary data

Supplementary data to this article can be found online at https://doi.org/10.1016/j.poly.2023.116469.

References

[1] B. Halliwell, J.M.C. Gutteridge, The importance of free radicals and catalytic metal ions in human diseases, Mol. Aspects Med. 8 (2) (1985) 89–193.
[2] W.W. Nawar, Lipids, in: O.R. Fennema (Ed.), Food Chemistry, 3rd ed., Marcel Dekker, New York, 1996, pp. 225–314.
[3] A. Shinde, J. Ganu, P. Naik, Effect of free radicals & Antioxidants on oxidative stress: a review, J. Dent. Allied Sci. 1 (2) (2012) 63–66.
[4] A. Schmidt, A. Beutler, B. Snovydovych, Recent advances in the chemistry of indazoles, Eur. J. Org. Chem. 2008 (24) (2008) 4073–4095.
[5] I. Denya, S.F. Malan, J. Joubert, Indazole derivatives and their therapeutic applications: a patent review (2013–2017), Expert Opin. Ther. Pat. 28 (6) (2018) 441–453.
[6] J. Dong, Q. Zhang, Z. Wang, G. Huang, S. Li, Recent advances in the development of indazole based anticancer agents, Chem. Med. Chem. 13 (15) (2018) 1490–1507.
[7] Bushra, S. Shamim, K.M. Khan, N. Ullah, M. Mahdavi, M.A. Faramarzi, B. Larijani, U. Salar, R. Rafique, M. Taha, S. Perveen, Perveen, Synthesis, in vitro, and in silico evaluation of Indazole Schiff bases as potential α-glucosidase inhibitors, J. Mol. Struct 1242 (2021) 130826.
[8] J. Elguero, A. Fruchier, E.M. Tjiou, S. Trofimenko, 13C NMR of indazoles, Chemistry of Heterocyclic Compounds 31 (9) (1995) 1006–1026.
[9] L. Mosti, G. Menozzi, P. Fossa, W. Filippelli, S. Gessi, B. Rinaldi, G. Falcone, Synthesis and preliminary biological evaluation of novel N-substituted 1-amino-3-[1- methyl (phenyl)-1H indazol 4- yloxy]-propan-2-ols interesting as potential antiarrhythmic, local anesthetic and analgesic agents, Arzneimittelforschung 50 (11) (2000) 963–972.
[10] N.A.S. Ali, B.A. Dar, V. Pradhan, M. Farooqui, Chemistry and biology of indoles and indazoles: amini-review, Mini Rev. Med. Chem. 13 (12) (2013) 1792–1800.
[11] Y.i. Wang, M.i. Yan, R. Ma, S. Ma, Synthesis and antibacterial activity of novel 4 bromo-1H indazole derivatives as FtsZ inhibitors, Arch. Pharm. Chem. Life Sci. 348 (4) (2015) 266–274.
[12] M. Gopalakrishnan, P. Sureshkumar, J. Thanusu, V. Kanagarajan, Synthesis, spectral analysis, antibacterial and antifungal activities of some 4,6-diaryl-4,5-dihydro-3-hydroxy-2[H]-indazole- a novel fused indazole derivative, J. Enzyme Inhib. Med. Chem. 23 (6) (2008) 974–979.
[13] S. Lin, F. Zhang, G. Jiang, S.A. Qureshi, X. Yang, G.G. Chicchi, L. Tota, A. Bansal, E. Brady, M. Trujillo, G. Salituro, C. Miller, J.R. Tata, B.B. Zhang, E.R. Parmee, A novel series of indazole-/indole-based glucagon receptor antagonists, Bioorg. Med. Chem. Lett. 25 (19) (2015) 4143–4147.
[14] H.C. Zhang, C.K. Derian, P. Andrade-Gordon, W.J. Hoekstra, D.F. McComsey, K. B. White, B.L. Poulter, M.F. Addo, W.M. Cheung, B.P. Damiano, D. Oksenberg, E. E. Reynolds, A. Pandey, R.M. Scarborough, B.E. Maryanoff, Discovery and optimization of a novel series of thrombin receptor (PAR-1) antagonists: potent, selective peptide mimetics based on indole and indazole templates, J. Med. Chem. 44 (7) (2001) 1021–1024.
[15] B. Thomas, K.S. Saravanan, P. Kochupurackal, K.P. Mohanakumar, In vitro and in vivo evidence that antioxidant action contributes to the neuroprotective effects of the neuronal nitric oxide synthase and monoamine oxidase-B inhibitor, 7-nitro indazole, Neurochem. Int. 52 (2008) 990–1001.

[16] H. Shirinzadeh, N. Altanlar, N. Yucel, S. Ozden, S. Suzen, Antimicrobial evaluation of indole containing hydrazone derivatives, Z. Naturforsch. C. J. Biosci. 66 (7–8) (2011) 340–344.
[17] L. Yurttaş, M. Ertaş, C. Yılmaz, M.Ş. Demirayak, Synthesis and antimycobacterial activity evaluation of isatin-derived 3- [(4-aryl-2-thiazolyl])hydrazone]-1H-indol-2,3-diones, Acta Pharm. Sci. 55 (1) (2017) 51–58.
[18] D.M. Martins, B.G. Torres, P.R. Spohr, P. Machado, H.G. Bonacorso, N. Zanatta, M.A. Martins, T. Emanuelli, Antioxidant potential of new pyrazoline derivatives to prevent oxidative damage, Basic Clin. Pharmacol. Toxicol. 104 (2008) 107–112.
[19] K. Karrouchi, L. Chemlal, L. Doudach, J. Taoufik, Y. Cherrah, S. Radi, M. E. Faouzi, M.H. Ansar, Synthesis, anti-inflammatory and antioxidant activities of some new pyrazole derivatives, J. Pharm. Res. 8 (8) (2014) 1171–1177.
[20] S. Viveka, Dinesha, L.N. Madhu, G.K. Nagaraja, Synthesis of new pyrazole derivatives via multicomponent reaction and evaluation of their antimicrobial and antioxidant activities, Monatsh Chem. 146 (9) (2015) 1547–1555.
[21] S. Durgamma, A. Muralikrishna, V. Padmavathi, A. Padmaja, Synthesis and antioxidant activity of amido-linked benzoxazolyl/benzothiazolyl/ benzimidazolyl-pyrroles and pyrazoles, Med. Chem. Res. 23 (6) (2014) 2916–2929.
[22] A. Rahman, S. Malik, S.S. Hasan, M.I. Choudhary, C.Z. Ni, J. Clardy, Nigellidine -a new indazole alkaloid from the seeds of Nigella sativa, Tetrahedron Lett. 36 (12) (1995) 1993–1996.
[23] M.S. Sigman, M.J. Schultz, The renaissance of palladium(II)-catalyzed oxidation chemistry, Org. Biomol. Chem. 2 (18) (2004) 2551–2554.
[24] F. Guarra, A. Pratesi, C. Gabbiani, T. Biver, A focus on the biological targets for coinage metal-NHCs as potential anticancer complexes, J. Inorg. Biochem. 217 (2021), 111355.
[25] S. Kankala, N. Thota, F. Bjorkling, M.K. Taylor, R. Vadde, R. Balusu, Silver carbene complexes: an emerging class of anticancer agents, Drug Dev. Res. 80 (2019) 188–199.
[26] N.F.H. Md Zin, S.Y.S. Ooi, B.-K. Khor, N.-Y. Chear, W.K. Tang, C.-K. Siu, M. R. Razali, R.A. Haque, W. Yam, Cytotoxicity of asymmetric mononuclear silver(I)-N-heterocyclic carbene complexes against human cervical cancer: synthesis, crystal structure, DFT calculations and effect of substituents, J. Organomet. Chem. 976 (2022) 122439.
[27] W.K. Jung, H.C. Koo, K.W. Kim, S. Shin, S.H. Kim, Y.H. Park, Antibacterial activity and mechanism of action of the silver ion in Staphylococcus aureus and escherichiacoli, Appl. Environ. Microbiol. 74 (7) (2008) 2171–2178.
[28] B.S. Atiyeh, M. Costagliola, S.N. Hayek, S.A. Dibo, Effect of silver on burn wound infection control and healing: review of the literatüre, Burns 33 (2) (2007) 139–148.
[29] M.L. Teyssot, A.S. Jarrousse, M. Manin, A. Chevry, F. Roche, F. Norre, C. Beaudoin, L. Morel, D. Boyer, R. Mahiou, A. Gautier, Metal-NHC complexes: a survey of anticancer properties, Dalton Trans. 35 (2009) 6894–6902.
[30] S. Hadjikakou, N. Hadjiliadis, N. Kourkoumelis, L. Kyros, M. Kubicki, M. Baril, I. S. Butler, S. Karkabounas, J. Balzarini, Tetrameric 1:1 and monomeric 1:3 complexes of silver(I) halides with tri(p-tolyl)-phosphine: a structural and biological study, Inorg. Chim. Acta. 362 (2009) 1003–1010.
[31] A. Gautier, F. Cisnetti, Advances in metal–carbene complexes as potent anti-cancer agents, Metallomics 4 (1) (2012) 23–32.
[32] C.N. Banti, D. GiannoulisA, N. Kourkoumelis, A.M. Owczarzak, M. Poyraz, M. Kubicki, K. Charalabopoulos, S.K. Hadjikakou, Mixed ligand–silver(i) complexes with anti-inflammatory agents which can bind to lipoxygenase and calfthymus DNA, modulating their function and inducing apoptosis, Metallomics 4 (2012) 545–560.
[33] S.M. Tailor, U.H.D.F.T. Patel, Study and Hirshfeld surface analysis of third polymorph of sulfamerazine, J. Coord. Chem. 68 (2015) 2192–2207.
[34] S.A. Patil, A.P. Hoagland, S.A. Patil, A. Bugarin, N-hetrocyclic carbine metal complexes as bioorganicmetallic antimicrobial and anticancer drugs, Future Med. Chem. 12 (24) (2020) 2239–2275.
[35] S. Celik, S. Yurdakul, B. Erdem, New silver(I) complex as antibiotic candidate: synthesis, spectral characterization, DFT, QTAIM and antibacterial investigations and docking properties, J. Mol. Struct. 1261 (2022), 132902.
[36] M. Yu, B. Liu, J. Guo, F. Wu, A sustainable modificatory 1, 2- alternate thiacalix [4]arene for detection of silver ion, Dyes Pigm. 210 (2023), 110983.
[37] S. Celik, S. Yurdakul, B. Erdem, Synthesis, spectroscopic characterization (FT-IR, PL), DFT calculations and antibacterial activity of silver(I) nitrate complex with nicotinaldehyde, Inorg. Chem. Commun. 131 (2021) 108760.
[38] H. Boulebd, S. Zama, B. Insaf, A. Bouraiou, S. Bouacida, H. Merazig, A. Romero, M. Chioua, J. Marco-Contelles, A. Belfaitah, Synthesis and biological evaluation of heterocyclic privileged medicinal structures containing (benz)imidazole unit, Monatsh. Chem. 147 (12) (2016) 2209–2220.
[39] D. Seenaiah, P.R. Reddy, G.M. Reddy, A. Padmaja, V. Padmavathi, N.S. Krishna, Synthesis, antimicrobial and cytotoxic activities of pyrimidinyl benzoxazole, benzothiazole and benzimidazole, Eur. J. Med. Chem. 77 (2014) 1–7.
[40] J.B. Patel, F.R. Cockerill, P.A. Bradford, Performance standards for antimicrobial susceptibility testing: twenty-fifth informational supplement. CLSI document M100–S25, Wayne, PA: Clinical and LAoratory Standards Institure (2015).
[41] K.H. McClean, M.K. Winson, L. Fish, A. Taylor, S.R. Chhabra, M. Camara, M. Daykin, J.H. Lamb, S. Swift, B.W. Bycroft, G.S.A.B. Stewart, P. Williams, Quorum sensing and Chromobacterium violaceum: exploitation of violacein production and inhibition for the detection of N-acylhomoserine lactones, Microbiology 143 (1997) 3703–3711.
[42] M.J. Frisch, G.W. Trucks, H.B. Schlegel, G.E. Scuseria, M.A. Robb, J.R. Cheeseman, G. Scalmani, V. Barone, B. Mennucci, G.A. Petersson, H. Nakatsuji, M. Caricato, X. Li, H.P. Hratchian, A.F. Izmaylov, J. Bloino, G. Zheng, J.L. Sonnenberg, M. Hada, M. Ehara, K. Toyota, R. Fukuda, J. Hasegawa, M. Ishida, T. Nakajima, Y. Honda, O. Kitao, H. Nakai, T. Vreven, J.A. Montgomery, Jr., J.E. Peralta, F. Ogliaro, M. Bearpark, J.J. Heyd, E. Brothers, K.N. Kudin, V.N. Staroverov, R. Kobayashi, J. Normand, K. Raghavachari, A. Rendell, J.C. Burant, S.S. Iyengar, J. Tomasi, M. Cossi, N. Rega, J.M. Millam, M. Klene, J.E. Knox, J.B. Cross, V. Bakken, C. Adamo, J. Jaramillo, R. Gomperts, R.E. Stratmann, O. Yazyev, A.J. Austin, R. Cammi, C. Pomelli, J.W. Ochterski, R.L. Martin, K. Morokuma, V.G. Zakrzewski, G.A. Voth, P. Salvador, J.J. Dannenberg, S. Dapprich, A.D. Daniels, O. Farkas, J.B. Foresman, J. V. Ortiz, J. Cioslowski, D.J. Fox, Gaussian, Inc., Wallingford CT, 2009.
[43] R. Dennington, T. Keith, J. Millam, GaussView, Version 5, Semichem Inc., Shawnee Mission, KS, 2009.
[44] J. Jebasingh Kores, I. Antony Danish, T. Sasitha, J. Gershom Stuart, E. Jimla Pushpam, J. Winfred Jebaraj, Spectral, NBO, NLO, NCI, aromaticity and charge transfer analyses of anthracene-9,10- dicarboxaldehyde by DFT, Heliyon 7 (11) (2021) e08377.
[45] N.S. Abdel-Kader, H. Moustafa, A.L. El-Ansaray, O.E. Sherifa, A.M. Farghalyb, A coumarin Schiff base and its Ag(i) and Cu(ii) complexes: synthesis, characterization, DFT calculations and biological applications, New. J. Chems. 45 (2021) 7714–7730.
[46] M.H. Jamroz, Vibrational energy distribution analysis (VEDA): scopes and limiations, Specrochim. Acta A 114 (2004) 220–230.
[47] K. Subashini, S. Periandy, Spectroscopic (FT-IR, FT-Raman, UV, NMR, NBO) investigation and molecular docking study of (R)- 2-Amino-1-PhenylEthanol, J. Mol. Struct. 1117 (2016) 240–256.
[48] A. Sadlej, J. Jaźwiński, Complexation in situ of 1-methylpiperidine, 1,2-dimethylpyrrolidin, and 1,2-dimethylpiperidine with rhodium(II) tetracarboxylates: nuclear magnetic resonance spectroscopy, chiral recognition, and density functional theory studies, Chirality 33 (10) (2021) 660–674.
[49] E. Polo, J. Trilleras, J. Ramos, A. Galdámez, J. Quiroga, M. Gutierrez, Efficient MW- assisted synthesis, spectroscopic characterization, X-ray and antioxidant properties of indazole derivatives, Molecules 21 (2016) 903.
[50] M.J. Mphahlele, N.M. Magwaza, S. Gildenhuys, I.B. Setshedi, Synthesis, α-glucosidase inhibition and antioxidant activity of the 7-carbo–substituted 5-bromo-3-methylindazoles, Bioor. Chem. 97 (2020) 103702.
[51] RSCB PDB Protein Data Bank. https://www.rcsb.org/. Accessed 01 January 2023.
[52] Biovia Visualization. https://www.3ds.com/products-services/ biovia/products/molecular-modeling-simulation/biovia-disco very-studio/visualization/. Accessed 01 January 2021.
[53] USCF Chimera https://www.cgl.ucsf.edu/chimera/. Accessed 01 January 2023.
[54] J.J.L. González, F.P. Ureña, J.R.A. Moreno, I. Mata, E. Molins, R.M. Claramunt, C. López, I. Alkorta, J. Elguerod, The chiral structure of 1H-indazoles in the solid state: a crystallographic, vibrational circular dichroism and computational study, New J. Chem. 36 (2012) 749–758.
[55] T.R. Fomuta, G. Djimassingar, J. Ngoune, N.O. Ngnabeuye, J.J. Anguile, J. Nenwa, Synthesis, structural characterization and DFT studies of silver(I) complex salt of bis(4,5-dihydro-1H-benzo[g]indazole), Cryst. Struct. Theory Appl. 6 (2017) 11–24.
[56] M. Govindarajan, K. Ganasan, S. Periandy, M. Karabacak, S. Mohan, Vibrational spectroscopic analysis of 2-chlorotoluene and 2-bromotoluene: a combined experimental and theoretical study, Spectrochim. Acta A: Mol. Biomol Spectrosc. 77 (2010) 1005–1013.
[57] S. Yurdakul, E. Temel, O. Büyükgüngör, Crystal structure, spectroscopic characterization, thermal properties and theoretical investigations on [Ag(methyl 4-pyridyl ketone)2NO3], J. Mol. Struct. 1191 (2019) 301–3013.
[58] R. Premkuma, R.M. Asath, T. Mathavan, A.M.F. Benial, Structural, vibrational spectroscopic and quantum chemical studies on indole-3-carboxaldehyde, AIP Publ. 140041 (2016) 1–3.
[59] M.A. El-Naggar, M.M. Sharaf, J.H. Albering, M.A.M. Abu-Youssef, T.S. Kassem, S. M. Soliman, A.M.A. Badr, One pot synthesis of two potent Ag(I) complexes with quinoxaline ligand: X- ray structure, Hirshfeld analysis, antimicrobial, and antitumor investigations, Sci. Rep. 12 (1) (2022).
[60] S.M. Soliman, A. Barakat, M.S. Islam, H.A. Ghabbour, Synthesis, crystal structure and DFT studies of a new dinuclear Ag(I)-malonamide complex, Molecules 23 (4) (2018) 888.
[61] C. Kucuk, S. Yurdakul, S. Celik, B. Erdem, Experimental and DFT studies of 2-methyl-quinoxaline and its silver (I) complex: Non-covalent interaction analysis, antimicrobial activity and molecular docking study, Inorg. Chem. Commun. 145 (2022) 109935.
[62] M.T. Bilkan, S. Yurdakul, Z. Demircioglu,-O. Büyükgüngor, Crystal structure, FT-IR, FT-Raman and DFT studies on a novel compound [C10H9N3]AgNO3, J. Organomet. Chem. 805 (2016) 108–116.
[63] A. Abdou, O.A. Omran, A. Nafady, I.S. Antipin, Structural, spectroscopic, FMOs, and non-linear optical properties exploration of three thiacaix(4)arenes derivatives, Arab. J. Chem. 15 (3) (2022), 103656.[62] J.A.P. Juniora, M. Cavicchioli, R.T.A. Machado, F.R. Pavan, D.H. Nakahata, P.P. Corbi, A.M.F. Costa, D.H. Pereira, A.C. Massabni, Synthesis, Characterization, DFT Modeling And In Vitro Antimycobacterial Activity Assays Of A Silver(I)-Isoniazid Complex, Quim. Nova.44(3) (2021), 278-283.
[64] J.A.P. Juniora, M. Cavicchioli, R.T.A. Machado, F.R. Pavan, D.H. Nakahata, P. P. Corbi, A.M.F. Costa, D.H. Pereira, A.C. Massabni, Synthesis, characterization, DFT modeling and in vitro antimycobacterial activity assays of a silver(I)-isoniazid complex, Quim. Nova. 44 (3) (2021) 278–283.
[65] L. Bučinský, G.E. Büchel, R. Ponec, P. Rapta, M. Breza, J. Kožíšek, M. Gall, S. Biskupič, M. Fronc, K. Schiessl, O. Cuzan, D. Prodius, C. Turta, S. Shova, D.

A. Zając, V.B. Arion, On the Electronic structure of mer, trans-[RuCl3(1H-indazole)2(NO)], a hypothetical metabolite of the antitumor drug candidate KP1019: an experimental and DFT study, Eur. J. Inorg. Chem. 14 (2013) 2505–2519.
[66] S.S. Khemalapure, V.S. Katti, C.S. Hiremath, S.M. Hiremath, M. Basanagouda, S. B. Radder, Spectroscopic (FT-IR, FT-Raman, NMR and UV-Vis), ELF, LOL, NBO, and Fukui function investigations on (5-bromo-benzofuran-3-yl)-acetic acid hydrazide (5BBAH): Experimental and theoretical approach, j, Mol. Struct. 1196 (2019) 280–290.
[67] S. Kumar, A. Radha, M. Kour, R. Kumar, A. Chouaih, S.K. Pandey, DFT studies of disubstituted diphenyldithiophosphates of nickel(II): structural and some spectral parameters, J. Mol. Struct. 1185 (2019) 212–218.
[68] Z. Demircioglu, C.A. Kastas, O. Büyükgüngor, The spectroscopic (FT-IR, UV-Vis), fukui function, NLO, NBO, NPA and tautomerism effect analysis of (E)-2-[(2-hydroxy-6- methoxybenzylidene)amino]benzonitrile, Spectrochim. Acta. A. 139 (2015) 539–548.
[69] H. Ebrahimi, J.S. Hadi, H.S. Al-Ansari, A new series of schiff bases derived from sulfa drugs and indole-3-carboxaldehyde: synthesis, characterization, spectral and DFT computational studies, J. Mol. Struct. 1039 (2013) 37–45.
[70] M.A. Mumit, T.K. Pal, M.A. Alam, M.A.A.A. Islam, S. Paul, M.C. Sheikh, DFT studies on vibrational and electronic spectra, HOMO–LUMO, MEP, HOMA, NBO and molecular docking analysis of benzyl-3N-(2,4,5-trimethoxyphenylmethylene) hydrazinecarbodithioate, J. Mol. Struct. 1220 (2020), 128715.
[71] H. Vural, M. Orbay, Synthesis, crystal structure, spectroscopic investigations and DFT calculations of the copper(II) complex of 4-(Trifluoromethyl)pyridine-2-carboxylic acid, J. Mol. Struct. 1146 (2017) 669–676.
[72] S.D. Oladipo, G.F. Tolufashe, C. Mocktar, B. Omondi, Ag(I) symmetrical N, N′-diarylformamidine dithiocarbamate PPh3 complexes: synthesis, structural characterization, quantum chemical calculations and in vitro biological studies, Inorg. Chim. Acta 520 (2021) 120316.
[73] F. Boursas, F. Berrah, N. Kanagathara, G. Anbalagan, S. Bouacida, Xrd, ft-ir,, FT-Raman spectra and ab initio HF vibrational analysis of bis (5-amino-3- carboxy-1H-1,2,4-triazol-4-ium) selenate dehydrate, J. Mol. Struct. 1180 (2019) 532e541.
[74] K. Sharma, R. Melavanki, S.S. Patil, R. Kusanur, N.R. Patil, V.M. Shelar, Spectroscopic behavior, FMO, NLO and NBO analysis of two novel aryl boronic acid derivatives: experimental and theoretical insights, J. Mol. Struct. 1181 (2019) 474e487.
[75] S. Xavier, S. Periandy, K. Carthigayan, S. Sebastian, Molecular docking, TG/DTA, molecular structure, harmonic vibrational frequencies, natural bond orbital and TD-DFT analysis of diphenyl carbonate by DFT approach, J. Mol. Struc. 1125 (2016) 204–216.
[76] F.B. Rizwana, J.C. Prasanaa, S. Muthu, C.S. Abraham, Molecular docking studies, charge transfer excitation and wave function analyses (ESP, ELF, LOL) on valacyclovir: a potential antiviral drug, Comput. Biol. Chem. 78 (2019) 9–17.
[77] B.R. Raajaraman, N.R. Sheela, S. Muthu, Spectroscopic, quantum computational and molecular docking studies on 1-phenylcyclopentane carboxylic acid, Comput. Biol. Chem. 82 (2019) 44–56.
[78] C. Morell, A. Grand, A. Toro-Labbé, New dual descriptor for chemical reactivity, J. Phys. Chem. A 109 (1) (2005) 205–212.
[79] B.Q. Sheeba, M.S.M. Mary, M. Amalanathan, C.B. Job, Structural and vibrational spectral investigation on the identification of Non-Linear Optical properties and wave function analyses (electrostatic potential, electron localisation function, localised orbital locator) of 3-Ethoxy Salicilaldehyde, Mol. Simul. 47 (15) (2021) 1217–1233.
[80] T. Lu, F. Chen, Multiwfn: a multifunctional wavefunction analyzer, J. Comput. Chem. 33 (5) (2012) 580–592.
[81] S. Murugavel, V.V. Velan, D. Kannan, M. Bakthadoss, Synthesis, crystal structure analysis, spectral investigations, DFT computations, biological activities and molecular docking of methyl(2E)-2-{[N-(2formlyphenyl)(4-metylbrnzene) sulfonamido]metyl}-3-(4-lurophenyl)prop-2enoate a potential bioactive agent, J. Mol. Struct. 1108 (2016) 150–167.
[82] R.F.W. Bader, M.A. Austen, Properties of atoms in molecules: atoms under pressure, J. Chem. Phys. 107 (11) (1997) 4271–4285.
[83] R.F.W. Bader, Atoms in Molecules : A. Quantum Theory, Oxford Univ. Press, 2, 1990.
[84] P.L.A. Popelier, F.M. Aicken, S.E. O'Brien, Atoms in Molecules, an Introduction, Prentice Hall, 2000, pp. 143–198.
[85] I. Rozas, I. Alkorta, J. Elguero, Behavior of ylides containing N, O, and C atoms as hydrogen bond acceptors, J. Am. Chem. Soc. 122 (45) (2000) 11154–11161.
[86] M. Saidj, A. Djafri, R. Rahmani, N.E.H. Belkafouf, N. Boukabcha, A. Djafri, A. Chouaih, Molecular Structure, Experimental and Theoretical Vibrational Spectroscopy, (HOMO-LUMO, NBO) Investigation, (RDG, AIM) Analysis, (MEP, NLO) Study and Molecular Docking of Ethyl-2-{[4-Ethyl-5-(Quinolin-8-yloxyMethyl)-4H-1,2,4-Triazol-3-yl] Sulfanyl} Acetate, Polycycl. Aromat, Compd, 2022.
[87] S. Jenkins, I. Morrison, The chemical character of the intermolecular bonds of sevenphases of ice as revealed by ab initio calculation of electron densities, Chem. Phys. Lett. 317 (1-2) (2000) 97–102.
[88] E. Espinosa, I. Alkorta, J. Elguero, E. Molins, From weak to strong interactions: a comprehensive analysis of the topological and energetic properties of the electron density distribution involving X-H F–Y systems, J. Chem. Phys. 117 (12) (2002) 5529–5542.
[89] A. Ramalingam, A.R. Guerroudj, S. Sambandam, A. Kumar, R. Krishnamoorthy, N. Boukabcha, A. Chouaih, M. Elayaperumal, Synthesis, vibrational spectra, Hirshfeld surface analysis, DFT calculations, and in silico ADMET study of 3-(2-chloroethyl)-2,6-bis(4-fluorophenyl)piperidin-4-one: A potent anti-Alzheimer agent, J. Mol. Struct. (2022, 1269,), 133845.
[90] B. Silvi, A. Savin, Classification of chemical bonds based on topological analysis of electron localization functions, Nature 371 (6499) (1994) 683–686.
[91] H. Jacobsen, Localized-orbital lacator (LOL) profiles of chemical bonding, Chan. J. Chem. 86 (2008) 695–702.
[92] S. Eryılmaz, N. Akdemir, E. İnkaya, The examination of molecular structure properties of 4,4′-oxydiphthalonitrile compound: combined spectral and computational analysis approaches, Spectrosc. Lett. 52 (1) (2019) 28–42.
[93] S.K. Gunduz, B. Bicak, S. Celik, S. Akyuz, A.e., Ozel Structural and spectroscopic investigation on antioxidant dipeptide, l-methionyl-l-serine: a combined experimental and DFT study, J. Mol. Struct. (2017, 1137,) 756–770.
[94] A. Sethi, R.P. Singh, D. Shukla, P. Singh, Synthesis of novel pregnane-diosgenin prodrugs via ring a and ring a connection: a combined experimental and theoretical studies, J. Mol. Struct. 1125 (2016) 616–623.
[95] J.B. Ott, J. Boerio-Goates Calculations from Statistical Thermodynamics, Academic Press, 2.
[96] S. Sangeetha Margreat, S. Ramalingam, S. Sebastian, S. Xavier, S. Periandy, J. C. Daniel, M. Maria Julie, DFT, spectroscopic, DSC/TGA, electronic, biological and molecular docking investigation of 2,5-thiophenedicarboxylic acid: a promising anticancer agent, J. Mol. Struct. (2020, 1200,), 127099.
[97] T. Joseline Beaula, I.H. Joe, V.K. Rastogi, V.B. Jothy, Spectral investigations, DFT computations and molecular docking studies of the antimicrobial 5-nitroisatin dimer, Chem. Phys. Letts. 624 (2015) 93–101.
[98] O.P. Sharma, T.K. Bhat, DPPH antioxidant assay revisited, Food Chemistry 113 (4) (2009) 1202–1205.
[99] R. Scherer, H.T. Godoy, Antioxidant activity index (AAI) by the 2,2-diphenyl-1-picrylhydrazyl method, Food Chem. 112 (3) (2009) 654–658.
[100] J. Deng, W. Cheng, G.A. Yang, Novel antioxidant activity index (AAU) for natural products using the DPPH assay, Food Chem. 125 (4) (2011) 1430–1435.
[101] E. Khan, Z. Gul, A. Shahzad, M.S. Jan, F. Ullah, M.N. Tahir, A. Noor, Coordination compounds of 4,5,6,7-tetrahydro-1H-indazole with Cu (II), Co (II) and Ag (I): structural, antimicrobial, antioxidant and enzyme inhibition studies, J. Coord. Chem. 70 (24) (2017) 4054–4069.
[102] W. Humphrey, A. Dalke, K. Schulten, VMD: visual molecular dynamics, J. Mol. Graphics 14 (1) (1996) 33–38.
[103] A.B. Lansdown, Silver in health care: antimicrobial effects and safety in use, Curr. Probl. Dermatol. 33 (2006) 17–34.
[104] J.G. Böttrich, F.H.H. Brill, J. Dissemond, J. Steinmann, K.C. Münter, F. Schümmelfeder, et al., A Systematic Review of the Risk of BacterialResistance to Silver, Poster, EWMA, 2018.
[105] S.L. Percival, E. Woods, M. Nutekpor, P. Bowler, A. Radford, C. Cochrane, Prevalence of silver resistance in bacteria isolated from diabeticfoot ulcers and efficacy of silver-containing wound dressings, Ostomy Wound Manag. 54 (3) (2008) 30–40.
[106] P. Kumari Patial, D. Sud, Bioactive phytosteroids from Araucaria columnaris (G. Forst.) Hook.: RP-HPLC-DAD analysis, in-vitro antioxidant potential, in-silico computational study and molecular docking against 3MNG and 1N3U, Steroids 188 (2022) 109116.
[107] W. Stadlbauer, Product Class 2: 1H and 2H- indazoles Sci Synth. 12(2002) 227-235.
[108] H. Cerecetto, A. Gerpe, M. González, V.J. Arán, C.O. de Ocáriz, Pharmacological properties of indazole derivatives: recent developments, Mini Rev. Med. Chem. 5 (2005) 869–878.
[109] B.R.K. Shyamlal, L. Yadav, M.K. Tiwari, M. Mathur, J.I. Prikhodko, I. V. Mashevskaya, S. Chaudhary, Synthesis, bioevaluation, structure-activity relationship and docking studies of natural product inspired (Z)-3-benzylideneisobenzofuran-1 (3H)-ones as highly potent antioxidants and antiplatelet agents, Sci. Rep. 10 (1) (2020) 2307.
[110] D. Seeliger, B.L. de Groot, Ligand docking and binding site analysis with Pymol and Autodock/Vina, J. Comput. Aided Mol. Des. 24 (5) (2010) 417–422.
[111] M. Kaur, R. Kaushal, Spectroscopic investigations, ab-initio DFT calculations, molecular docking and in-vitro assay studies of novel oxovanadium(V)chalcone complexes as potential antidiabetic agents, J. Mol. Struct. 1271 (2023), 133994.
[112] A. Hameed, M. al-Rashida, M. Uroos, S. Abid Ali, K.M. Khan, Schiff bases in medicinal chemistry: a patent review (2010–2015), Expert Opin. Ther. Pat. 27 (1) (2017) 63–79.